IEEE Access
Multidisciplinary | Rapid Review | Open Access Journal

Received July 11, 2018, accepted August 25, 2018, date of publication September 5, 2018, date of current version October 8, 2018.

Digital Object Identifier 10.1109/ACCESS.2018.2868863

Dynamic Response and Parametric Analysis of Geometrically Nonlinear Functionally Graded Plate With Arbitrary Constraints Under Moving Mass

QINGHUA SONG[1,2], YUN QIN[1], ZHANQIANG LIU[1,2], JIAHAO SHI[1,3], AND BING WANG[1]

[1]Key Laboratory of High Efficiency and Clean Mechanical Manufacture, Ministry of Education, School of Mechanical Engineering, Shandong University, Ji'nan 250061, China
[2]National Demonstration Center for Experimental Mechanical Engineering Education, Shandong University, Ji'nan 250061, China
[3]Department of Bioresource Engineering, McGill University, Ste-Anne-de-Bellevue QC H9X 3V9, Canada

Corresponding author: Qinghua Song (ssinghua@sdu.edu.cn)

The authors are grateful to the financial supports of the National Natural Science Foundation of China (Grants 51575319 and 51875320), Young Scholars Program of Shandong University (Grant 2015WLJH31), the United Fund of Ministry of Education for Equipment Pre-research (Grant 6141A02022116), and the Key Research and Development Plan of Shandong Province (Grant 2018GGX103007).

ABSTRACT A comprehensive method is presented to investigate nonlinear dynamic responses of functionally graded rectangular plate with arbitrary boundary conditions under a moving mass, based on Rayleigh–Ritz solutions together with the penalty method (PM) and the Newmark with inverse Broyden quasi-Newton method. Different from the existing methods, all inertial effects associated with the moving mass, which affect the mass, damping, and stiffness matrices of system, are taken into account. The formulations are derived based on classical plate theory and von Kármán geometric nonlinearity, which considers large deformation without violating stress failure criteria. Material properties of FG plate vary continuously in the thickness direction according to the power law. The PM is employed to deal with the troublesome arbitrary constraints, which excludes an orthonormalization process for determining these admissible functions, and where only one set of admissible functions is used for arbitrary boundary conditions. The Newmark method together with the rank-one inverse Broyden quasi-Newton method is adopted to solve the nonlinear coupled differential equations of second order in time with more computational efficiency and avoiding numerical instability. Formulation and method of solution are validated by studying their convergence behavior and performing the comparison studies with existing results in the literature in the limit cases. In addition, influences of different material distribution, velocity of moving mass, different conventional, and unconventional boundary conditions on forced and free vibration responses are discussed.

INDEX TERMS Functionally graded plate, nonlinear response, moving mass, penalty method, arbitrary boundary conditions.

I. INTRODUCTION

With the intensive research efforts during the last several decades, large spectrums of high technology materials are available today. As novel advanced materials in the family of engineering composites, functionally graded materials (FGMs) are made of two or more constituent phases with continuously and smoothly varying composition [1]. Compared with homogeneous material composed of similar constituents, the material properties of FGM can be adjusted in the preferred direction/orientation to meet the specific requirements in different engineering applications. These desired performances can be achieved by varying the volume fraction of the constituent materials. These excellent advantages have made it possible for the century's most astonishing technological achievements in the fields of mechanical [2], aerospace [3], optoelectronics [4], biomedical [5], and other engineering applications.

As important elements in several complex structures, FGMs are always made for beams, plates and shells. Therefore, it is of great importance to study the dynamic behaviors

of FGM structural elements so as to design effective and strong structural elements for building durability and yet cost optimized structures. Nguyen *et al.* [6] obtained the natural frequencies and vibration modes of thin-walled I- and channel-sections FG beams. Wang *et al.* [7] investigated free vibration of a bi-direction functionally graded beam. As for rectangular plates, Baferani *et al.* [8] found an exact analytical solution for free vibration characteristics of thin FG rectangular plates with different boundary conditions. Mantari *et al.* [9] used Carrera unified formulation with five new displacement fields of the non-polynomial form to analyze the static characteristic of FG single and sandwich plate. The dynamic analysis of FG plate based on a novel first shear deformation theory (FSDT) [10] and quasi-3D and 2D shear deformation theories [11] were also conducted.

Moving load problems, which are one of the most important problems in the structural dynamics, have been studied for well over a century. For large deformation, the nonlinear vibration analysis of different FG beams was conducted, where von Kármán geometric nonlinearity with Euler-Bernoulli beam theory or Timoshenko beam theory was used to derive the system's energy equations [12], [13]. For moving load of large mass, Simsek [14] took the inertial effects of moving mass including the centripetal and Coriolis effects into consideration. Other moving mass problems of axially and bi-directional FG beams were also proposed [15], [16]. Similar with the moving mass problems of FG beams, the responses of FG plate and shell subjected to moving load were also analyzed by many researchers. Akbarzadeh *et al.* [17] studied the mechanical behavior of FG rectangular plate based on the FSDT and the third-order shear deformation theory with a lateral mechanical load on its upper surface. The transverse vibrations and stability of a moving skew FG plate were investigated in oblique coordinate system by the method of coordinate transformation [18]. Malekzadeh and Monajjemzadeh [19] studied the nonlinear response of FG plate subjected to moving load with constant speed. FEM in conjunction with Newmark's time integration scheme and Newton–Raphson method were employed to solve the system with different boundary conditions. Mamandi *et al.* [20] also presented the nonlinear dynamic analysis of a simple supported rectangular plate subjected to an accelerated/decelerated moving mass/force. Besides moving load, some nonlinear responses of FG shells and plates subjected to immovable time varying loads were studied [21], [22]. Additionally, the topic of dynamic analysis of FGM structures in thermal environment has also continuously attracted great attention of many researchers [23]–[25]. However, only temporal inertial component (i.e., simplified partial time derivative) associated with the moving mass was considered in the most studies mentioned above, while the convective inertial components were ignored, except for Rofooei *et al.*'s works [26], where conventional nonlinear method (i.e., total Lagrangian technique) together with Newmark-Beta method was employed to study the dynamic response of rectangular plate including the all inertial effects induced by moving mass. Meanwhile, the restrictions of conventional finite element (FE) codes were reviewed in [26], e.g., required very fine mesh for accuracy results in extremely time consuming, only weight and transverse inertial component (i.e., simplified moving mass effect) of moving mass would be considered with neglecting all other inertial components because of the nature of Contact-Target elements used in codes to present the interaction between main structure and moving mass.

Most of the studies on the vibration analysis of FG structure elements are with classical boundary conditions, such as free edges, simply supported, or clamped. In real systems while there are some derivations from the ideal boundary conditions, and it is quite hard to find the ideal constraints. As a result of this demand, some unconventional boundary conditions should be considered to analyze the dynamic characteristics of the FG beams, plates and shells. However, a large number of studies on FG structure elements have been confined to classical constraints, studies on FG structure elements with unconventional conditions and the methods to deal with them are very rare. Najafizadeh *et al.* [27] modeled one edge of FG plate with non-ideal constraints where there was a small non-zero deflection and moment. In [28]–[30], the natural frequency and modal shape of FG plates resting on elastic foundation were obtained. Similarly, Simsek and Cans?z [31] studied the dynamic response of an elastically connected double-functionally graded beam system subjected to a moving harmonic load with some classical boundary conditions. However, point constraint was assumed in the form of supports to be linear springs of large stiffness. Simsek [14] adopted Lagrange multiplier method to treat the simple-supported boundary condition, where the space-dependent polynomial terms were selected as x0, x1,..., xN-1 and Lagrange multipliers were used to reflect the constraint. In addition, Sari and Butcher [32] and Wattanasakulpong and Mao [33] proposed the model of FG beams with damaged boundary condition. In these literatures, boundary damage factors were adopted, which allows for a wide range of boundary conditions between fixed (i.e. undamaged) and free ends. Apart from damage boundary, Gupta *et al.* [34] established a model of FG plate with mixed boundary condition. The results were accomplished by employing a C0 continuous isoparametric finite element formulation.

The above reviews clearly indicate that there are two critical issues need to be investigated extensively. One is the inertial effect of moving mass, especially the convective inertial components are notably significant when the weight of moving mass becomes considerable in comparison with the main structure's mass [26]. In this regard, the moving mass inertial effects were restricted only to the weight and simplified moving mass effect in the most of the existing studies. The other is that the majority of the aforementioned works focused on the dynamic analysis of FG structure elements with classical boundary conditions. Further, the works [27]–[30] and [32]–[34] related to vibration analysis

of FG beams and FG plates with unconventional constraints were limited to obtain the linear natural frequency and modal shape, while the process to solve the nonlinear transient response of moving load problem was more difficult. Also, in the works [27]–[30], [32], and [33], these unconventional boundary conditions were uniformly distributed along the edge of the plates or concentrated on one end of the beams. For the mixed boundary condition in [34], the FEM was used to avoid finding the proper spatial function. However, this mixed boundary condition was still similar to the uniformly distributed constraint to some degree when it comes to certain area of the edge.

Therefore, based on the above reviews, there is a strong encouragement to gain an understanding of the all inertial effects of moving mass and the vibration response of unconventional constrained structure, as well as the mathematical modeling of such phenomena. As a first endeavor, this paper focuses on the nonlinear dynamic behaviors of unconventional constrained FG rectangular plate subjected to a moving mass based on classical plate theory (CPT) and von Kármán geometric nonlinearity, which is not available in the open literatures. To deal with the troublesome unconventional constraints, penalty method (PM) is adopted. The equations of motion are derived with the aid of Lagrange's equations, where the pseudo-mass, pseudo-damping and pseudo-stiffness effects are presented obviously to reveal the all inertial effects of moving mass. To avoid the numerical instability, the Newmark method together with rank-one inverse Broyden quasi-Newton method (N-IBQNM) is employed to find the nonlinear dynamic responses of FG plate. Finally, the influences of different material distribution, velocity of moving mass, different conventional and unconventional boundary conditions on forced and free vibration responses are presented in detail.

II. THEORETICAL FORMULATIOINS

A. DEFINITIONS OF GEOMETRY AND MATERIAL PROPERTIES

Figure1 shows a thin FG plate with length L, width W and thickness h, which is subjected to a moving mass (M) traveling on an arbitrary trajectory on its surface.

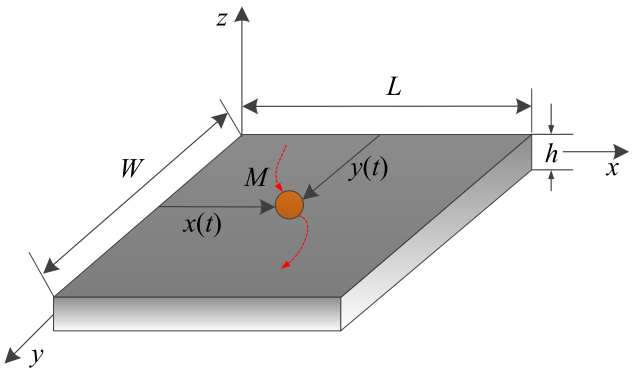

FIGURE 1. Model of FG plate under moving mass.

Although the method is capable of solving the dynamic problem for nonlinear FG rectangular plates with arbitrary mass moving trajectories, only rectilinear trajectories are considered here to avoid unnecessary complexity. Without loss of generality of the formulation and the method of solution, the material properties of a ceramic-metal FG plate are assumed to vary continuously through the thickness. The material points of the FG plate with unstressed reference configuration are labelled in a Cartesian coordinate system (x, y, z). The displacement components of an arbitrary material point (x, y, z) of the plate are denoted as $\bar{u}$, $\bar{v}$, and $\bar{w}$ along the x, y, and z-directions, respectively.

As mentioned previously, the effective material properties of the FG plate are obtained according to the rule of mixture. Here, the power-law (or Mori-Tanaka model) [34] is adopted as,

$$P(z) = P_m + (P_c - P_m)\left(V_f\right)^p, \quad p \geq 0 \tag{1}$$

where the subscripts m and c refer to the metal and ceramic constituents, respectively. p is the power law index or the material property graded index, and V_f $(=\frac{2z+h}{2h})$ is the ceramic volume fraction.

B. CONSTITUTIVE RELATIONSHIPS

Due to the large length-to-thickness ratio of thin plate, the classical plate theory (CPT) based on Kirchhoff hypothesis, seems to be sufficient for modeling of the dynamic response of this type of plate. Accordingly, the variation of displacement components $\bar{u}$, $\bar{v}$, and $\bar{w}$ of an arbitrary material point of FG plate are approximated along the thickness direction as, respectively,

$$\begin{aligned} \bar{u}(x, y, z, t) &= u(x, y, t) - zw_{,x} \\ \bar{v}(x, y, z, t) &= v(x, y, t) - zw_{,y} \\ \bar{w}(x, y, z, t) &= w(x, y, t) \end{aligned} \tag{2}$$

where, u, v, and w represent the displacement components of the material point (x, y) on the mid-plane along the x, y and z-directions, respectively. $(\,)_{,x}$ and $(\,)_{,y}$ represent the partial differentiations with respect to x and y, respectively.

Using the nonlinear Green's strain tensor together with von Kármán assumptions [35], the nonzero strain (i.e., Green-Lagrange strain) tensor components at an arbitrary material point (x, y, z) of the FG plate can be expressed in terms of the displacement components of the material point (x, y) on the mid-plane as,

$$\begin{aligned} \varepsilon_{xx} &= u_{,x} + \frac{1}{2}w_{,x}^2 - zw_{,xx} \\ \varepsilon_{yy} &= v_{,y} + \frac{1}{2}w_{,y}^2 - zw_{,yy} \\ 2\varepsilon_{xy} &= u_{,y} + v_{,x} + w_{,x}w_{,y} - 2zw_{,xy} \end{aligned} \tag{3}$$

where $(\,)_{,xx}$, $(\,)_{,xy}$, and $(\,)_{,yy}$ represent the second-order partial derivatives with respect to x and y, respectively. Also, based on the plane stress assumption, the nonzero components of the stress (i.e., the 2nd Piola-Kirchhoff stress) tensor at an

TABLE 1. Stiffnesses of extension spring and torsion spring for classical boundary conditions.

Boundary condition	Diagram	Geometrical relationship	Stiffness		Diagram
			k_t	k_r	
F	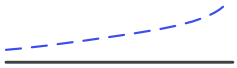	$w \neq 0, \frac{\partial w}{\partial x} \neq 0$	0	0	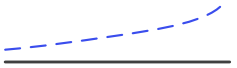
S	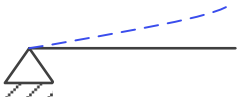	$w = 0, \frac{\partial w}{\partial x} \neq 0$	P	0	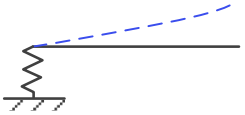
C	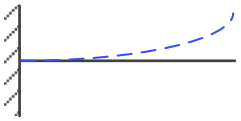	$w = 0, \frac{\partial w}{\partial x} = 0$	P	P	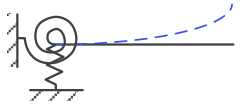
G	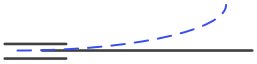	$w \neq 0, \frac{\partial w}{\partial x} = 0$	0	P	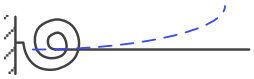

arbitrary material point of the FG plate can be expressed in terms of the displacement components as,

$$\begin{aligned}
\sigma_{xx} &= \frac{E(z)}{(1-\mu^2)}\left[u_{,x} + \mu v_{,y} + \frac{1}{2}w_{,x}^2 + \frac{\mu}{2}w_{,y}^2 \right. \\
&\qquad \left. - z\left(w_{,xx} + \mu w_{,yy}\right)\right] \\
\sigma_{yy} &= \frac{E(z)}{(1-\mu^2)}\left[\mu u_{,x} + v_{,y} + \frac{\mu}{2}w_{,x}^2 + \frac{1}{2}w_{,y}^2 \right. \\
&\qquad \left. - z\left(\mu w_{,xx} + w_{,yy}\right)\right] \\
\sigma_{xy} &= G(z)\left(u_{,y} + v_{,x} + w_{,x}w_{,y} - 2zw_{,xy}\right) \qquad (4)
\end{aligned}$$

where E, G, and μ are Young's modulus, the shear rigidity and Poisson's ratio of the FG plate, respectively.

C. RAYLEIGH-RIZE SOLUTION WITH PENALTY METHOD FOR ARBITRARY BOUNDARY CONDITIONS

From (2)-(4), it can be seen that only three unknown displacement parameters are needed to determine the total energy of the FG plate. Considering the restrains of available FE programs aforementioned, here Rayleigh-Ritz method (RRM) is used to approximately express the displacement components,

$$\begin{aligned}
v &= \sum_{i=1}^{N}\sum_{j=1}^{N} q_{ij}(t)\phi_i(x)\varphi_j(y) \\
v &= \sum_{i=1}^{N}\sum_{j=1}^{N} q_{ij}(t)\phi_i(x)\varphi_j(y) \\
w &= \sum_{i=1}^{N}\sum_{j=1}^{N} w_{ij}(t)\phi_i(x)\varphi_j(y) \qquad (5)
\end{aligned}$$

where w_{ij}, p_{ij}, and q_{ij} are Ritz coefficients (or modal coordinates) and $\phi_i(x)$ and $\varphi_j(y)$ are admissible functions.

In conventional RRM, the choosing of admissible functions and the accuracy of the approximation are the two main difficulties. These problems arise mainly because of the need to satisfy the geometrical constraints of a specific system, which makes the derivation of governing equation very complex and complicated. For some unconventional boundary conditions, such as local restrictions, it will be more difficult to find proper admissible functions. To study the nonlinear responses of FG plate under different boundary conditions and provide a general process of deriving governing equation for different boundary conditions, in this paper, the penalty method (PM) is employed to handle constraints, and the admissible functions adopted here just satisfy a totally unconstrained condition, thereby avoiding the process of finding suitable admissible functions for different boundary conditions. That is, only one set of admissible functions is used for arbitrary boundary conditions. The spirit of this method is the use of artificial stiffness or concentrated mass with very large magnitude so that a rigid constraint could be approximately modeled by a constraint [36], [37]. Therefore, the higher the stiffness of the spring or the concentrated mass, which may be referred to as a penalty parameter, the harder it is to violate the constraint. Based on this spirit, the stiffness PM, inertial PM and bi-PM were proposed. The stiffness PM is easier to understand and acceptable to replace different constraint, so this typical PM is employed here. To realize this method, extension spring and torsion spring are adopted to constrain the translation and bend, respectively. Normally, the penalty parameter is taken as 1×10^9 (N/m or N/rad). Table 1 lists the combination of the stiffnesses of extension spring, k_t, and torsion spring, k_r, for four classical boundary conditions (F-free, S-simply supported, C-clamped and G-guided), where P is penalty parameter value.

As known, trigonometric functions and hyperbolic functions are generally used to be as the admissible functions. However, the solutions presented using these functions are slow to convergence, and the most admissible functions are associated with constraints, that is, different sets of admissible functions are necessary for different

boundary conditions. On the other side, polynomials are commonly applied to express the displacement solutions [38]. However, high order polynomials are the cause of numerical instabilities and ill-conditioning, so the combination of polynomials and trigonometric functions seems to be the best choice. To improve the numerical stability and convergent rate, the following admissible functions, satisfying the totally unconstrained condition, are adopted

$$\phi_i(x) = \begin{cases} \left(\frac{x}{L}\right)^{i-1}, & i = 1, 2, 3 \\ \cos\frac{(i-3)\pi x}{L} & i = 4, 5, \ldots, N \end{cases}$$

and

$$\varphi_j(y) = \begin{cases} \left(\frac{y}{W}\right)^{j-1} & j = 1, 2, 3 \\ \cos\frac{(j-3)\pi y}{W} & j = 4, 5, \ldots, N \end{cases} \tag{6}$$

It should be emphasized that, an orthonormalization process is commonly required to obtain the proper admissible functions, such as Gram-Schmidt procedure is widely used to generate the orthogonal polynomials satisfying the appropriate boundary conditions in boundary characteristic orthogonal polynomials (BCOPs) [38]. However, the orthonomalization process isn't included here to determine admissible functions due to PM, so the present method can be used to deal with arbitrary boundary conditions avoid employing different admissible functions associated with different constraints.

D. ENERGY FORMULATIONS

The kinetic energy of plate, T, can be expressed as

$$\begin{aligned} T &= \frac{1}{2}\iint_A \int_{-h/2}^{h/2} \rho(z)\left(\dot{\bar{w}}^2 + \dot{\bar{u}}^2 + \dot{\bar{v}}^2\right) dz dA \\ &= I_0 \iint_A \left(\dot{w}^2 + \dot{u}^2 + \dot{v}^2\right) dA - 2I_1 \iint_A \left(\dot{u}\dot{w}_{,x} + \dot{v}\dot{w}_{,y}\right) dA \\ &\quad + I_2 \iint_A \left(w_{,y}^2 + w_{,x}^2\right) dA \end{aligned} \tag{7}$$

where $\dot{(\cdot)}$ is partial derivatives with respect to time, and I_0, I_1, and I_2 are defined as

$$I_i = \frac{1}{2}\int_{-h/2}^{h/2} \rho(z) z^i dz, \quad i = 0, 1, 2 \tag{8}$$

The potential energy, U, of plate is

$$\begin{aligned} U &= E_0 \iint_A \left[\left(u_{,x} + \frac{1}{2}w_{,x}^2\right)^2 + \left(v_{,y} + \frac{1}{2}w_{,y}^2\right)^2 \right. \\ &\quad \left. + \frac{(1-\mu)}{2}\left(u_{,y} + v_{,x} + w_{,x}w_{,y}\right)^2\right] dA \\ &\quad - 2E_1 \iint_A \left[w_{,xx}\left(u_{,x} + \frac{1}{2}w_{,x}^2\right) + w_{,yy}\left(v_{,y} + \frac{1}{2}w_{,y}^2\right) \right. \\ &\quad \left. + 2(1-\mu)w_{,xy}\left(u_{,y} + v_{,x} + w_{,x}w_{,y}\right)^2\right] dA \\ &\quad + E_2 \iint_A \left[w_{,xx}^2 + w_{,yy}^2 + 2(1-\mu)w_{,xy}^2\right] dA \\ &\quad + 2E_0 \iint_A \left[\mu\left(u_{,x} + \frac{1}{2}w_{,x}^2\right)\left(v_{,y} + \frac{1}{2}w_{,y}^2\right)\right] dA \\ &\quad - 4E_1 \iint_A \left[\mu w_{,xx}\left(v_{,y} + \frac{1}{2}w_{,y}^2\right) + \mu w_{,yy} \right. \\ &\quad \left. \times \left(u_{,x} + \frac{1}{2}w_{,x}^2\right)\right] dA + E_2 \iint_A \left(2\mu w_{,xx}w_{,yy}\right) dA \end{aligned} \tag{9}$$

where E_0, E_1, and E_2 are defined as

$$E_i = \frac{1}{2(1-\mu^2)}\int_{-h/2}^{h/2} E(z) z^i dz, \quad i = 0, 1, 2 \tag{10}$$

In (9), the first three terms mean linear part of the potential energy of plate, while the last three terms stand for the nonlinear part of the plate's potential energy due to large deformation. If these terms were ignored, the final equation derived from (9) would be the linear governing equation of FG plate. And, the potential energy of moving mass, W, can be expressed as (11), as shown at the bottom of this page.

In the brace of (11), there are seven distinct terms to introduce the inertial effects induced by the moving mass. The first term is the weight of mass, Mg, which corresponds to the moving load problem (see (A.10) in **Appendix**). For the case of moving mass problem, while the other six terms influence the overall mass, damping and stiffness matrices of system (as shown in (13)). That is, the second term corresponding to the simplified moving mass effect influences the mass matrix (see (A.2) in **Appendix**), and the third, fourth and fifth terms determine the stiffness matrix (see (A.6) in **Appendix**), and the last two terms corresponds to the damping matrix (see (A.4) in **Appendix**). Noted that here the in-plane moving acceleration terms ($\ddot{u}_{ij}$ and $\ddot{v}_{ij}$) of mass are neglected due to the constant or lower moving velocity hypothesis. If these two terms were added, there would be nine distinct terms in the brace of (11), which are consistent with those presented in [26]. In fact, these terms which affect the stiffness matrix, are generally ignored for response of thin plate due to the weaker effect than that of transverse acceleration ($\ddot{w}_{ij}$).

It should be also mentioned that, due to the introduction of virtual spring, the additional strain energy arising from the

$$\begin{aligned} W &= -\iint_A \left[Mg + M\ddot{w}_0\left(x_0(t), y_0(t), t\right)\right]\delta(x - x_0)\delta(y - y_0)w_0(x_0, y_0, t)dA \\ &= -M\left\{g + \sum_{i=1}^{N}\sum_{j=1}^{N}\begin{bmatrix} \ddot{w}_{ij}(t)\phi_i(x_0)\varphi_j(y_0) + 2\dot{x}_0\dot{y}_0 w_{ij}(t)\phi_{i,x}(x_0)\varphi_{j,y}(y_0) \\ +\dot{x}_0^2 w_{ij}(t)\phi_{i,xx}(x_0)\varphi_j(y_0) + \dot{y}_0^2 w_{ij}(t)\phi_i(x_0)\varphi_{j,yy}(y_0) \\ +2\dot{x}_0\dot{w}_{ij}(t)\phi_{i,x}(x_0)\varphi_j(y_0) + 2\dot{y}_0\dot{w}_{ij}(t)\phi_i(x_0)\varphi_{j,y}(y_0) \end{bmatrix}\right\} \times \sum_{i=1}^{N}\sum_{j=1}^{N}\left[w_{ij}(t)\phi_i(x_0)\varphi_j(y_0)\right] \end{aligned} \tag{11}$$

translational and rotational springs should be considered and expressed as $V = V_w + V_u + V_v$. Here

$$V_J = \frac{1}{2}\left(k_{1,\mathrm{t}}^J \int_0^W J^2\Big|_{x=0} dy + k_{1,\mathrm{r}}^J \int_0^W J_{,x}^2\Big|_{x=0} dy + k_{2,\mathrm{t}}^J \int_0^L J^2\Big|_{y=0} dx + k_{2,\mathrm{r}}^J \int_0^L J_{,x}^2\Big|_{y=0} dx \right) + \frac{1}{2}\left(k_{3,\mathrm{t}}^J \int_0^W J^2\Big|_{x=L} dy + k_{3,\mathrm{r}}^J \int_0^W J_{,y}^2\Big|_{x=L} dy + k_{4,\mathrm{t}}^J \int_0^L J^2\Big|_{y=W} dx + k_{4,\mathrm{r}}^J \int_0^L J_{,y}^2\Big|_{y=W} dx \right) \quad (12)$$

where, $J = w, u, v$. $k_{,\mathrm{t}}^J$ and $k_{,\mathrm{r}}^J$ are stiffness coefficients of the translational and rotational springs and determined by the boundary conditions. It is noted that, the unconventional boundary conditions can be easily achieved by changing the range of integration and stiffness coefficients. For example, to satisfy the mixed boundary condition of F and S, it just needs to divide the integral interval according to different constraint ranges, while the corresponding stiffness coefficient is determined by its boundary condition.

E. GOVERNING EQUATION OF MOTION

For this system presented previously, the Lagrange is $L = T\text{-}U\text{-}V\text{-}W$. The governing equation of motion of the system can be obtained by using Lagrange's equation, and expressed as

$$\begin{bmatrix} \mathbf{M}_{11}+\mathbf{M}_{11}^* & \mathbf{M}_{12} & \mathbf{M}_{13} \\ \mathbf{M}_{21} & \mathbf{M}_{22} & \mathbf{0} \\ \mathbf{M}_{31} & \mathbf{0} & \mathbf{M}_{33} \end{bmatrix} \begin{Bmatrix} \{\ddot{w}\} \\ \{\ddot{p}\} \\ \{\ddot{q}\} \end{Bmatrix} + \begin{bmatrix} \mathbf{C}_{11}^* & \mathbf{0} & \mathbf{0} \\ \mathbf{0} & \mathbf{0} & \mathbf{0} \\ \mathbf{0} & \mathbf{0} & \mathbf{0} \end{bmatrix} \times \begin{Bmatrix} \{\dot{w}\} \\ \{\dot{p}\} \\ \{\dot{q}\} \end{Bmatrix} + \begin{bmatrix} \mathbf{K}_{11}+\mathbf{K}_{11}^* & \mathbf{K}_{12} & \mathbf{K}_{13} \\ \mathbf{K}_{21} & \mathbf{K}_{22} & \mathbf{K}_{23} \\ \mathbf{K}_{31} & \mathbf{K}_{32} & \mathbf{K}_{33} \end{bmatrix} \begin{Bmatrix} \{w\} \\ \{p\} \\ \{q\} \end{Bmatrix} + \{\mathbf{f}(\{w\},\{p\},\{q\})\}^{NL} = \begin{Bmatrix} \{F\} \\ \{0\} \\ \{0\} \end{Bmatrix} \quad (13)$$

where $\mathbf{0}$ is $N \times N$ zero matrix, $\{w\}=[w_{11}\ w_{12}\ \ldots\ w_{1N}\ w_{21}\ \ldots\ w_{NN}]^T$, $\{p\}=[p_{11}\ p_{12}\ \ldots\ p_{1N}\ p_{21}\ \ldots\ p_{NN}]^T$, $\{q\}=[q_{11}\ q_{12}\ \ldots\ q_{1N}\ q_{21}\ \ldots\ q_{NN}]^T$. Matrices $\mathbf{M}_{11}^*$, $\mathbf{C}_{11}^*$ and $\mathbf{K}_{11}^*$, known as pseudo-mass, pseudo-damping and pseudo-stiffness matrices, are caused by the moving mass, all of which are functions of time and correspond to the later six terms in the brace of (11). All these sub-matrices are listed in **Appendix**. The influences of different inertia components on natural frequencies, responses and stability have been revealed using the prepared nonlinear FE codes in [26]. Therefore, the paper moves the emphasis on the dynamic responses of nonlinear FG plate subjected a moving mass with arbitrary constraints including all the inertial effects. As shown in (8) and (10), due to the properties of the FG plate, I_0, I_1, I_2, E_0, E_1, and E_2 are all non-zero value. Correspondingly, the noted sub-matrices are also all non-zero matrices. However, for isotropic plate, due to its constant value of density and elasticity modulus along the thickness, both I_1 and E_1 are of zero value. Therefore, sub-matrices $\mathbf{M}_{12}$, $\mathbf{M}_{13}$, $\mathbf{M}_{21}$, $\mathbf{M}_{31}$, $\mathbf{K}_{12}$, $\mathbf{K}_{13}$, $\mathbf{K}_{21}$, and $\mathbf{K}_{31}$ degrade to null matrix. It also should be emphasized that the first three terms in the left side of (13) are responsible for linear response of the plate, while the fourth term, $\{\mathbf{f}(\{w\},\{p\},\{q\})\}^{NL}$, of $(3 \times N \times N) \times 1$, are aroused from the nonlinear part of potential energy of the plate. Therefore, neglecting the fourth term on the left side of (13), this governing equation of motion degenerates to linear equation for calculating the linear response of FG plate. For convenience of the following calculation, the fourth term is rewritten in the following form

$$\{\mathbf{f}(\{w\},\{p\},\{q\})\}^{NL} = \mathbf{K}^{NL} \begin{Bmatrix} \{w\} \\ \{p\} \\ \{q\} \end{Bmatrix} = \begin{bmatrix} \mathbf{K}_{11}^{NL}(\{w\}) & \mathbf{0} & \mathbf{0} \\ \mathbf{K}_{21}^{NL}(\{w\}) & \mathbf{0} & \mathbf{0} \\ \mathbf{K}_{31}^{NL}(\{w\}) & \mathbf{0} & \mathbf{0} \end{bmatrix} \begin{Bmatrix} \{w\} \\ \{p\} \\ \{q\} \end{Bmatrix} \quad (14)$$

where the sub-matrices in (14) are also listed in **Appendix**. Noted that the nonlinear stiffness matrix $\mathbf{K}^{NL}$ is not unique and can have different forms, which only need to satisfy (14).

When the traveling mass leaves the plate, some correlative items equal to zero, such as $\mathbf{M}_{11}^* = \mathbf{C}_{11}^* = \mathbf{K}_{11}^* = \mathbf{0}$ and $\{F\}=\{0\}$. Thus, the solution of (13) represents the nonlinear free vibration of the FG plate in this case.

Additionally, equation (13) can also be written in the compact form

$$\mathbf{M}\{\ddot{y}\} + \mathbf{C}\{\dot{y}\} + \mathbf{K}\{y\} + \mathbf{K}^{NL}(\{y\})\{y\} = \{Q\} \quad (15)$$

where matrices $\mathbf{M}$, $\mathbf{C}$, $\mathbf{K}$, and $\mathbf{K}^{NL}$ are of order $(3 \times N \times N) \times (3 \times N \times N)$. $\{y\}$ and $\{Q\}$ are general modal vector and force vector, and expressed as

$$\{y\} = \underbrace{\left\{\{w\}^T, \{p\}^T, \{q\}^T\right\}^T}_{(3\times N^2)\times 1} \text{ and } \{Q\} = \underbrace{\left\{\{F\}^T, \{0\}^T, \{0\}^T\right\}^T}_{(3\times N^2)\times 1} \quad (16)$$

F. RESPONSES ANALYSIS

Mathematically, equation (15) is a system of nonlinear coupled ordinary differential equations of second-order in time, which can be solved using various explicit or implicit time step methods. However, as mentioned in [26], it is very challenging to achieve numerical stability for this kind of equations due to the variable kinematic parameters (such as variable mass, damping and stiffness matrices). Newmark-Beta method (known as constant average acceleration method) was employed to numerical solve the equation derived in [26]. To avoid the numerical instability and deal with the nonlinear terms in equation with more computational efficiency, therefore the constant-average acceleration method from Newmark's time integration family in conjunction with rank-one inverse Broyden quasi-Newton method (IBQNM) is employed here to solve (15) and determine the dynamic response of the plate at any time instant.

With Newmark's time integration scheme, equation (15) is transformed into a set of nonlinear algebraic equations in the following form

$$\bar{\mathbf{K}}^e(y_{s+1})y_{s+1} = \bar{\mathbf{F}}^e_{s+1} \tag{17}$$

where the subscript $s+1$ for a variable means the value of that variable at the time $t = t_{s+1}$. $\bar{\mathbf{K}}^e(y_{s1})$ and $\bar{\mathbf{F}}^e_{s,s+1}$ are the effective stiffness matrix and the load vector, respectively, which according to Newmark's scheme can be expressed as

$$\begin{aligned}\bar{\mathbf{K}}^e(y_{s+1}) &= a_0\mathbf{M}_{s+1} + a_1\mathbf{C}_{s+1} + \mathbf{K}_{s+1} + \mathbf{K}^{NL}(y_{s+1})\\ \bar{\mathbf{F}}^e_{s+1} &= \{\mathbf{F}_{s+1}\} + \mathbf{M}_{s+1}\left(a_0 y_s + a_2\dot{y}_s + a_3\ddot{y}_s\right)\\ &\quad + \mathbf{C}_{s+1}\left(a_1 y_s + a_4\dot{y}_s + a_5\ddot{y}_s\right)\end{aligned} \tag{18}$$

where

$$\begin{aligned}&a_0 = \frac{1}{\gamma dt^2}, \quad a_1 = \frac{\beta}{\gamma dt}, \; a_2 = \frac{1}{\gamma dt}, \; a_3 = \frac{1}{2\gamma} - 1,\\ &a_4 = \frac{\beta}{\gamma} - 1, \quad a_5 = \frac{dt}{2}\left(\frac{\beta}{\gamma} - 2\right), \; a_6 = dt(1-\beta),\\ &a_7 = \beta dt\end{aligned} \tag{19}$$

where dt is the time step and based on the constant-average acceleration method the values of $\gamma = 0.25$ and $\beta = 0.5$ should be used, in which condition the solution will be of unconditional convergence [40].

Since the effective stiffness matrix $\bar{\mathbf{K}}^e(y_{s+1})$ is a nonlinear function of the generalized modal coordinates y_{s+1}, an iterative solution procedure is needed to solve (17) at each time step. As mentioned previously, rank-one IBQNM is adopted here, which is of more computational efficiency than the commonly used Broyden quasi-Newton method and Newton–Raphson method [39]. The important feature of this method is that it deals with the updating of the inverse of the effective stiffness matrix and not with the effective stiffness matrix itself.

According to this method, at any time step,

$$y_{i+1} = y_i - B_i Z(y_i) \tag{20}$$

where i is the iteration number, and

$$Z(y_i) = \bar{\mathbf{K}}^e(y_i)y_i - \bar{\mathbf{F}}^e_i \tag{21}$$

$$B_{i+1} = B_i - \frac{(B_i q_i - p_i)\,(p_i)^T B_i}{(p_i)^T B_i q_i} \tag{22}$$

here

$$p_i = y_{i+1} - y_i \text{ and } q_i = Z(y_{i+1}) - Z(y_i) \tag{23}$$

As can be seen from (22), the above computation involves only matrix multiplication at each step, which improves the computational efficiency of solving this nonlinear algebraic equation. To start the procedure we need an initial approximation y_0 and B_0. In this paper, the y_0 is taken as zero vector of $(3\times N\times N)\times 1$ and B_0 is unit matrix of $(3\times N\times N)\times(3\times N\times N)$. Then at each iteration, according to (20), y is updated. This procedure is continued until the difference between two successive solution vectors is less than a selected tolerance criterion, i.e.,

$$\sqrt{\frac{(y_{i+1}-y_i)^T(y_{i+1}-y_i)}{y_i^T y_i}} \le 10^{-4} \tag{24}$$

where the superscript T means the transpose of a vector or matrix.

After achieving the convergence, the general modal vector y at time $t = t_{i+1}$ is obtained, and consequently, the new acceleration vector $\ddot{y}$ and the new velocity vector $\dot{y}$ at time $t = t_{i+1}$ are computed from the following equations, respectively,

$$\ddot{y}_{i+1} = a_0(y_{i+1} - y_i) - a_2\dot{y}_i - a_3\ddot{y}_i \tag{25}$$

For the next time step, all the steps mentioned above should be repeated to evaluate the general modal vector, acceleration vector, and velocity vector. In this study, all models, calculation procedures and required analysis are performed and accomplished using MATLAB software.

III. CONVERGENCE AND ACCURACY

Before conducting parametric analysis of FG plate, the convergence and accuracy of present method are estimated. The calculated results by the proposed method are compared with those given in published literatures for the following two examples, respectively. Since the information regarding the nonlinear response of FG plate under moving mass is not available, the plate with isotopic material is considered here.

A. MODAL ANALYSIS

Firstly, the convergence and accuracy of the proposed method are verified based on the natural characteristic analysis. Here, the linear non-dimensional frequency parameters, $\omega = \varpi L^2\sqrt{12\rho(1-\mu^2)/Eh^3}$, of an isotopic square plate are calculated and compared with the results given in [8]. Based on (1), when the power law index equals to zero, the FG plate degenerates into isotopic plate made of the ceramic constituents. In this case, all of matrices $\mathbf{M}^*_{11}$, $\mathbf{C}^*_{11}$, and $\mathbf{K}^*_{11}$ are zero as well as both nonlinear terms $\{\mathbf{f}\}^{NL}$ and force vector $\{F\}$ are zero in (13). All Stiffness coefficient combinations used are listed in Table 2. The boundary conditions mentioned in the following sections include SSSS, FSFS, SSFS, FCFF, SSXF, and SF$\bar{S}$F.

The natural frequencies of the plate can be obtained by solving the characteristic equation of (13) with these assumptions mentioned above. Table 3 gives the non-dimensional frequency parameters of the plate with penalty parameters changing from 10^3 to 10^9. It is evident that the present results are in excellent agreement with those generated in [8]. It is also clear that the performance of the present method is better in terms of solution accuracy when the penalty parameters are larger than 10^7. In order to get accurate results, the penalty parameter is selected as 10^9 in this paper, that is $P = 1\times 10^9$ in Table 2.

TABLE 2. Stiffness coefficient combinations for four edges with different boundary conditions.

	Edge	F			S			C			$\bar{S}$		
		w	u	v	w	u	v	w	u	v	w	u	v
k_t	(1)	0	0	0	P	P	P	P	P	P	$y{\cdot}k$	$y{\cdot}k$	$y{\cdot}k$
	(2)	0	0	0	P	P	P	P	P	P	$x{\cdot}k$	$x{\cdot}k$	$x{\cdot}k$
	(3)	0	0	0	P	P	P	P	P	P	$y{\cdot}k$	$y{\cdot}k$	$y{\cdot}k$
	(4)	0	0	0	P	P	P	P	P	P	$x{\cdot}k$	$x{\cdot}k$	$x{\cdot}k$
k_r	(1)	0	P	P	0	0	0	P	0	0	0	0	0
	(2)	0	P	P	0	0	0	P	0	0	0	0	0
	(3)	0	P	P	0	0	0	P	0	0	0	0	0
	(4)	0	P	P	0	0	0	P	0	0	0	0	0

TABLE 3. Influences of penalty parameters on the non-dimensional frequency parameters for six boundary conditions isotopic plate (in Hz).

Penalty parameters	SSSS			SCSC			SFSF		
	ω_{11}	ω_{12}	ω_{13}	ω_{11}	ω_{12}	ω_{13}	ω_{11}	ω_{12}	ω_{13}
10^3	18.12	42.97	79.00	25.27	51.85	81.32	9.41	15.04	35.91
10^5	19.70	49.24	98.45	28.91	69.10	128.36	9.63	16.10	36.62
10^7	19.74	49.35	98.70	28.95	69.33	129.10	9.63	16.13	36.72
10^9	19.74	49.35	98.70	28.95	69.33	129.10	9.63	16.13	36.73
[8]	19.74	49.35	98.70	28.95	69.32	129.09	9.63	16.13	36.72
Penalty parameters	SSSC			SCSF			SSSF		
	ω_{11}	ω_{12}	ω_{13}	ω_{11}	ω_{12}	ω_{13}	ω_{11}	ω_{12}	ω_{13}
10^3	21.31	47.73	80.44	12.06	29.22	58.78	11.18	25.15	54.62
10^5	23.61	58.49	112.76	12.67	32.98	72.19	11.67	27.69	61.71
10^7	23.65	58.65	113.23	12.69	33.06	72.39	11.68	27.75	61.86
10^9	23.65	56.65	113.23	12.69	33.07	72.40	11.69	27.76	61.86
[8]	23.65	58.64	113.22	12.69	33.06	72.40	11.68	27.76	61.86

B. RESPONSE ANALYSIS

In this example, the convergence and accuracy of the provided method are verified through response analysis. Similar with the descriptions presented previously, a simple supported 2m×2m square isotropic plate with a modulus of $E = 71$GPa, mass density $\rho = 2700$kg/m^3, 1cm thickness and Poisson's ratio $\mu = 0.33$ is used. The moving mass trajectory is assumed to be parallel to x axis passing through the middle of the plate. The moving mass velocity, v_m, is seen as constant.

The dynamic response of the plate undergoing a moving mass is generally described by its center point time history amplitude that is normalized with respect to its static deflection. Thus, the dynamic amplification factor (DAF), which is defined as the ratio of the dynamic displacement of the plate to its static deflection at its center point, is used to present the dynamic responses. The static deflection of the center point of a simple supported square plate subjected to a concentrated mass M, located at the same position is equal to $\Delta_{\text{static}} = 0.0116 M_r M_{\text{plate}} g L^2/D$ [35], where g is the gravitational acceleration, M_{plate} is the mass of the FG plate, and M_r is the mass ratio of the moving mass to the plate.

Figures 2 and 3 show convergences of the DAFs of center point for the prescribed plate subjected to a moving mass with mass ($M_r = 0.2$) and velocity ($v_m = 9.852$m/s). All the time are normalized with respect to the contacting time t_f ($= L/v_m$) during which the mass moves on the plate. Therefore, as separated with a red dashed line, all these response diagrams can be divided into two parts: forced vibration and free vibration. The first part corresponds to the period in which the mass contacts with the plate, while the second part occurs due to the separation between them. It can be seen from Fig. 2, no matter what the number of Ritz terms N is, the converging trend of solutions with decrease of the time step size, which results in the increase of the number of the adopted time points, is obvious. It is not difficult to find that time ratios Δt of 10×10^{-3} and 5×10^{-3} are small enough to get the convergent results, where the time ratio Δt is defined as the ratio of the time step size dt used in the Newmark method, to the contacting time t_f. A similar converging trend also can be found in Fig. 3 with increasing of Ritz terms (N) and the use of only 7-8 Ritz test functions are sufficient to achieve accurate solution.

Table 4 shows the accuracy and convergence of the maximum DAFs of the previous responses. The calculated results with different Ritz terms and time step sizes are compared with those given by [35]. A similar conclusion can be made that when $N \geq 7$ and $\Delta t \leq 10 \times 10^{-3}$, the results are in good

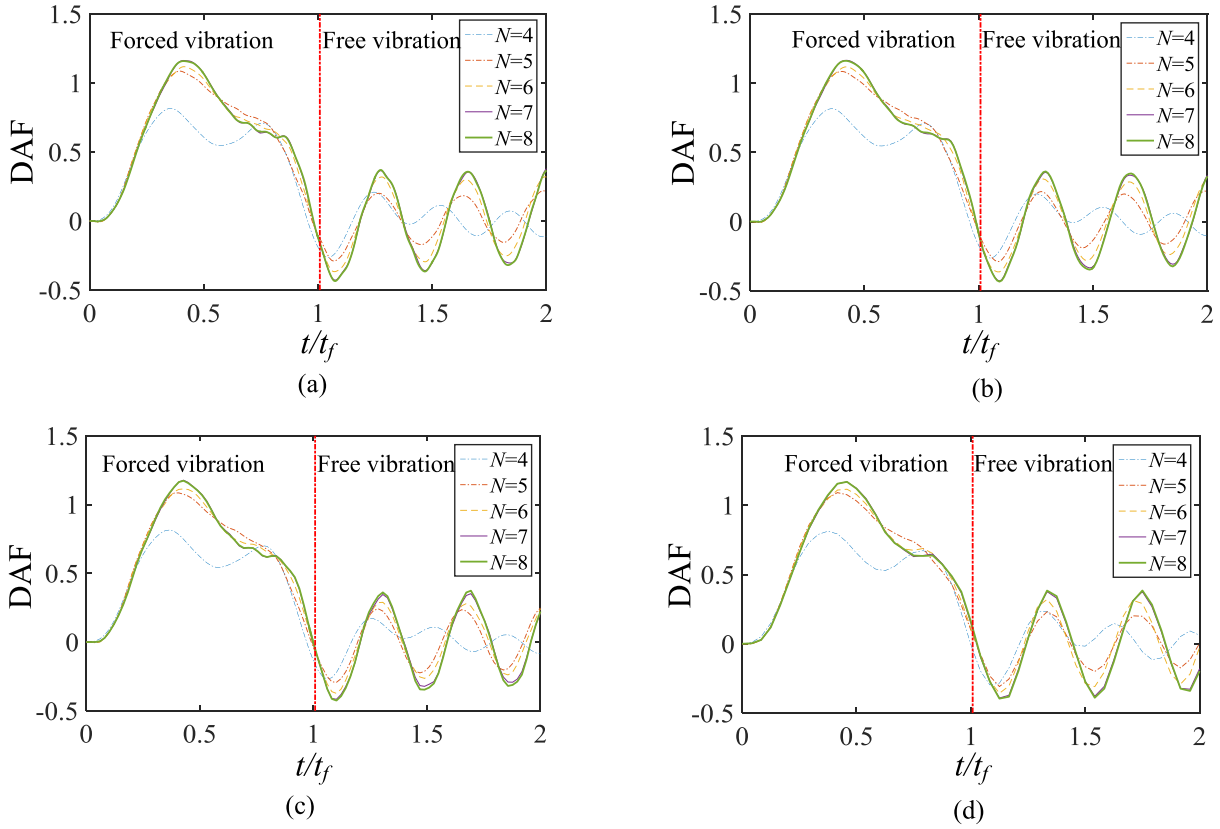

FIGURE 2. Convergence of DAF time history of center point for a simple supported isotropic plate subjected to a moving mass with respect to time ratio. (a) $\Delta t = 5 \times 10^{-3}$. (b) $\Delta t = 10 \times 10^{-3}$. (c) $\Delta t = 20 \times 10^{-3}$. (d) $\Delta t = 40 \times 10^{-3}$.

TABLE 4. Maximum DAFs of center point of a simple supported isotropic plate subjected to a moving mass with M_r=0.2 (M=21.6kg) and v_m=9.852m/s.

Δt	DAF					
	N=4	N=5	N=6	N=7	N=8	[35]
5×10^{-3}	0.815	1.086	1.118	1.163	1.167	1.166
1×10^{-2}	0.815	1.085	1.118	1.165	1.166	
2×10^{-2}	0.815	1.084	1.114	1.177	1.173	
4×10^{-2}	0.813	1.091	1.116	1.169	1.169	

agreement with the ones got in [35]. Therefore, considering the accuracy of the solution and the amount of the calculation, here the Ritz terms and time ratio are compromised and taken as 7 and 10×10^{-3}, respectively.

IV. PARAMETRIC ANALYSIS

After being satisfied about the validity of the solution technique, FG plates with arbitrary boundary conditions are discussed, and the instantaneous dynamic vertical deflection of central point of plate is calculated in the following section. In the all solved examples, otherwise specified, the following parameters are used: $L = W = 1$m, $h = 0.01$m, $N = 7$, and $\Delta t = 10 \times 10^{-3}$. The moving velocity of mass is constant, and the moving path is $y = W/2$. For FG plate, material properties of ZrO_2 (ceramic) and aluminum (metal), given in Table 5, are used in numerical calculations. Noted that here the mass ratio M_r is defined as the ratio of moving mass to mass of aluminum plate which is of the same size with the FG plate. For the sake of brevity, a counterclockwise notation starting from $x = 0$ is utilized to identify the boundary conditions of the plate; for example, the symbol 'CSFC' represents a plate with the clamped edge (C) at $x = 0$, simply supported (S) at $y = W$, free (F) at $x = L$ and clamped (C) at $y = 0$.

TABLE 5. Material properties of ZrO_2 (ceramic) and aluminum (metal).

Material	Elasticity modulus (GPa)	Poisson's ratio	Density (kg/m^3)
ZrO_2	200	0.3	5700
Al	70	0.3	2700

Here, in contrast to the classical boundary conditions, the arbitrary boundary conditions mean that the constraint

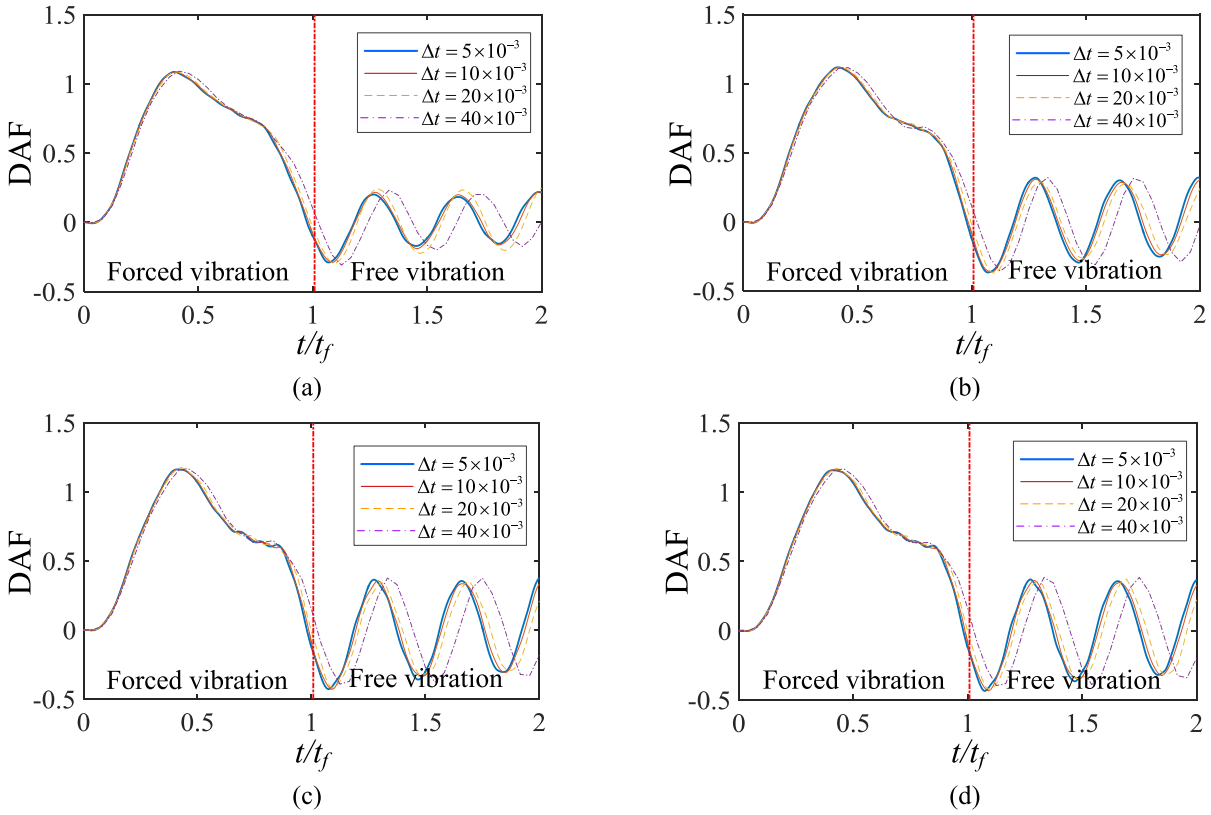

FIGURE 3. Convergence of DAF time history of center point for a simple supported isotropic plate subjected to a moving mass with respect to Ritz terms. (a) $N = 5$. (b) $N = 6$. (c) $N = 7$. (d) $N = 8$.

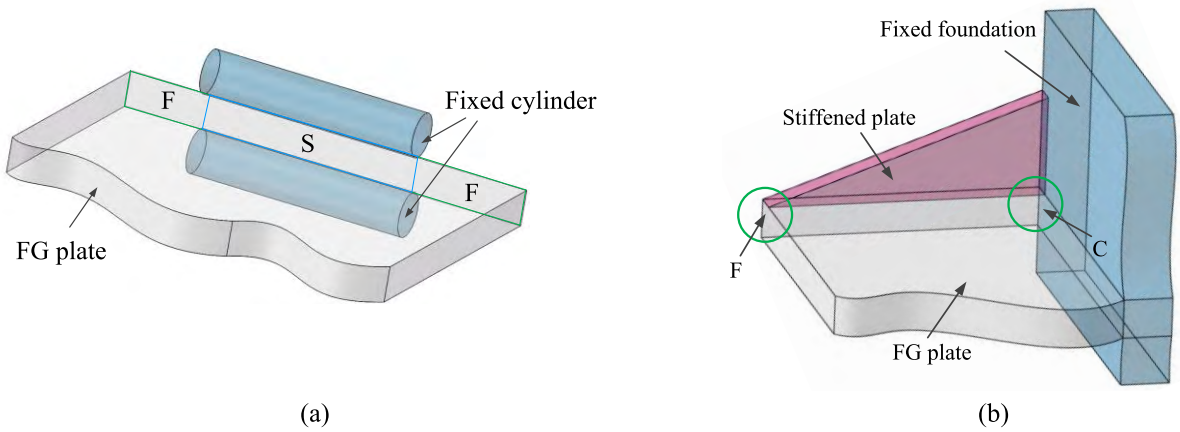

FIGURE 4. FG plate with arbitrary boundary conditions. (a) Partly simple supported plate. (b) Triangular stiffened plate.

is unevenly distributed along the same edge. In this case, it is hard to find a suitable function to satisfy this kind of boundary condition. However, by adopting the penalty method, the admissible functions just need to satisfy a totally unconstrained condition while the artificial spring is used to deal with the constraint. Without loss of generality, two kinds of arbitrary boundary conditions are analyzed here. In the first one, one edge of the plate is partly simple supported while the other place of this edge is free, as shown in Fig. 4(a). In the second case, the constraint varies linearly along one edge of the plate, such as the triangular stiffened plate shown in Fig. 4(b).

In open literatures [34], [41]–[45], some studies are available in which free vibration analysis of square plate with mixed boundary conditions has been observed, which are valuable for basic understanding. In general, there is no numerical solution of forced vibration of functionally graded material plate with mixed boundary conditions are available

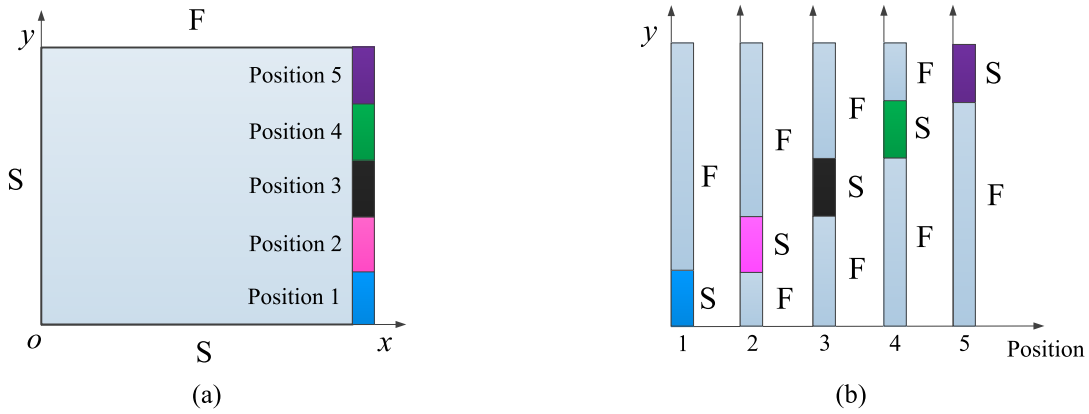

FIGURE 5. FG plate with SSXF. (a) Local constrained FG plate. (b) Constraints with different positions (Edge 3).

TABLE 6. Maximum DAFs during forced vibration period and free vibration period for FG plate with five different local constraint positions and M_r=1, p=2.

v_m	SSFF		Position 1		Position 2		Position 3		Position 4		Position 5	
(m/s)	Forced	Free	Forced	Free	Forced	Free	Forced	Free	Forced	Free	Forced	Free
10	**5.2754**	**5.1436**	1.3668	0.7154	0.7905	0.2472	0.6769	0.1180	0.6361	0.0415	0.6592	0.1507
20	3.2315	4.1085	**1.9131**	**1.8328**	1.2288	0.7592	1.1270	0.5921	1.0828	0.4649	1.1081	0.3495
30	2.0744	3.3746	1.9057	1.5802	1.6928	1.5255	1.6023	1.3463	1.4646	1.1613	1.3870	1.2526
40	1.1240	2.6787	1.3259	1.4245	**1.8133**	**1.9056**	**2.1115**	2.2190	**1.9012**	1.9123	1.6040	1.5799
50	1.0584	2.7249	1.2516	1.5113	1.6339	1.8705	1.9801	**2.4708**	1.8100	**2.1823**	**1.6050**	1.7334
60	1.1539	2.9491	1.2744	1.4710	1.4304	1.7582	1.6756	2.4577	1.4874	1.9998	1.3422	1.8755
70	1.1766	2.4782	1.2230	1.4096	1.2227	1.6727	1.3799	2.3272	1.1747	1.8836	1.1004	1.9488
80	1.1480	1.7770	1.1056	1.2619	1.0058	1.5387	1.1079	2.1548	0.9413	1.7442	0.9552	1.9605
90	1.1038	1.3764	0.9844	1.2240	0.8153	1.3835	0.8775	1.9538	0.7742	1.6038	0.8813	1.9823

as per the authors' knowledge. Therefore, some computed results are shown here by using the present computational approach for the vibration characteristics of FG plate.

A. LOCAL CONSTRAINT WITH DIFFERENT POSITIONS

Firstly, the local constraint with different positions is considered. As shown in Fig. 5a, along the edge $x = 1$m (Edge 3), five places, namely 0∼0.2m (Position 1), 0.2∼0.4m (Position 2), 0.4∼0.6m (Position 3), 0.6∼0.8m (Position 4) and 0.8∼1m (Position 5), are partly simple supported, which share the same constraint size and the other parts of the edge are in free. Therefore, this unconventional constraint can be seen as a mix of simple supported boundary condition and free boundary condition. For the sake of brevity, 'X' is used to represent the local constraint. For example, the boundary condition shown in Fig. 5(a) is expressed as SSXF. The corresponding penalty parameters are listed in Table 2. It should be mentioned that the integral in (10) should be divided into different parts since the penalty parameters have different values along the Edge 3. Fig. 5(b) describes the constraint distribution along Edge 3. It can be seen that the free boundary condition dominates the most place of the edge. Therefore, this unconventional SSXF is similar as the classical SSFF.

Figure 6 depicts the center point responses ((a)-(c)) and forced vibration responses ((d)-(f)) of the contacting points with $M_r = 1$, $p = 2$ and $v_m = 20$m/s. From Fig. 6(a)-(c), it can be seen that when t/t_f is smaller than 0.5, there is little difference for the center point responses with five different local constraint positions. When this value exceeds 0.5, the gap between these responses is enlarged. This is due to the effect of the constraints in edge $x = 0$ m (Edge 1) dominating the center point response in the beginning. As the mass moves away from $x = 0$m, the impact of local constraints becomes more important. A similar phenomenon can also be found in Fig. 6(d)-(f). From the results shown in Fig. 6, one can clearly see the effect of local constraint position, i.e., as the local constraint closes to the Edge 4 ($y = 1$m), such as Position 5, center point response and dynamic response are all mitigated. This effect is because when the local constraint closes to the x axis, the simple supported edge, $y = 0$m, has more influence on the response of plate while the effect of local constraint (i.e., Position 1) can be neglected. On the contrary, for Position 5, with free boundary condition in Edge 4, the local constraint can totally display its ability of constraint. It also can be observed that the displacements in z direction ((a) and (d)) are much larger than those in x and y directions ((b), (c), (e), and (f)), which means more attention should be paid to the traverse displacement.

In Tables 6 and 7, the maximum DAF during force vibration period and free vibration period for FG plate with local constraint distributed in five different positions are listed. The power law index p is 2 and the mass ratios M_r are 0.2 and 1, respectively. From the data of Table 6, the effect of configuration position on critical speed is easy to be observed. For both

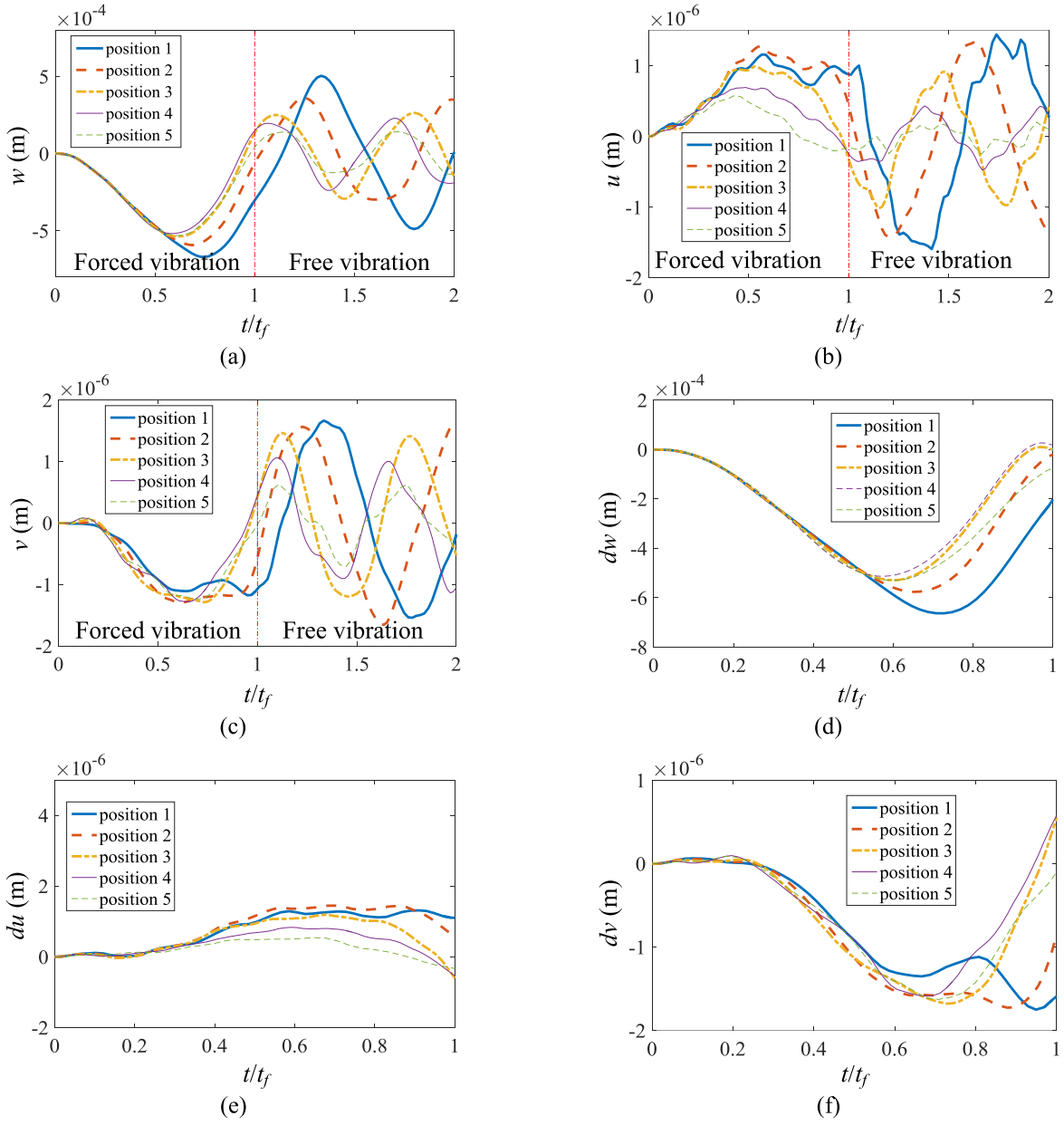

FIGURE 6. Responses of FG plate subjected to moving mass with five different local constraint positions and M_r=1, p=2, v_m=20m/s. (a), (b), and (c) tie history for center point responses; (d), (e) and (f) forced vibration responses of the contacting points.

forced and free vibrations, their critical speeds all increase when the configuration moves from $y = 0$m (Position 1) to $y = 1$m (Position 5). For example, the critical speeds of both forced vibration and free vibration for Position 1 are 20m/s. However, when it comes to Position 5, the critical speed of forced vibration increases to 50m/s, while that for free vibration exceeds 90m/s. Another interesting result is that when comparing the Maximum DAFs of SSFF and SSXF with size of 0.2m, this value with SSXF reduces significantly. For example, even for Position 1 and with the critical speed of the SSXF plate, the maximum DAF decreases from 3.23 to 1.91 for forced vibration, and 4.11 to 1.83 for free vibration, which means even small local constraints can provide high performance of vibration suppression. Similar results are also found in Table 7. Comparing Table 6 with Table 7, it is clear that increasing the mass ratio from 0.2 to 1 not always results in improvements of the critical speed.

Figure 7 gives the maximum three-dimension deformations of FG plate at critical speed with $M_r = 1$ and $p = 2$. It is clear that the local constraint position has significant effect on the shape and the magnitude of deformation of plate. With local constraint configured in Position 1, the maximum deformation is maximum (about 2.5mm), and only few areas near the edge $x = 1$m is restricted. With the local restriction

TABLE 7. Maximum DAFs during forced vibration period and free vibration period for FG plate with five different local constraint positions and M_r=0.2, p=2.

v_m	SSFF		Position 1		Position 2		Position 3		Position 4		Position 5	
(m/s)	Forced	Free	Forced	Free	Forced	Free	Forced	Free	Forced	Free	Forced	Free
10	3.5261	3.5637	1.2701	0.9561	0.7195	0.0964	0.6655	0.1507	0.6837	0.1727	0.7164	0.3107
20	**4.2906**	**5.4353**	1.6333	1.4254	1.0168	0.3039	0.9034	0.0974	0.8765	0.1557	0.8794	0.2986
30	2.4546	4.1033	**1.6942**	**1.7185**	**1.0808**	0.8174	1.0102	0.7404	1.0313	0.5933	1.0469	0.6349
40	1.2449	3.0312	1.0770	1.5023	0.9703	0.9504	**1.0242**	0.8093	1.0985	0.9237	1.1407	1.0102
50	0.8103	2.3191	0.8480	1.5653	0.8998	**1.0301**	0.9950	**0.9852**	**1.1172**	1.0485	**1.1806**	1.0868
60	0.8009	2.1467	0.8742	1.5678	0.9227	0.8497	0.9735	0.9750	1.0883	**1.1288**	1.1480	**1.1648**
70	0.7853	2.0132	0.8940	1.5278	0.9579	0.9331	0.9933	0.9660	1.0071	1.0343	0.9834	1.1330
80	0.7653	1.6203	0.8980	1.4373	0.9741	0.9820	0.9942	0.9617	0.9288	0.9700	0.8261	1.0815
90	0.7410	0.9903	0.8628	1.0416	0.9353	0.9855	0.9543	0.9528	0.8550	0.9148	0.7288	1.0168

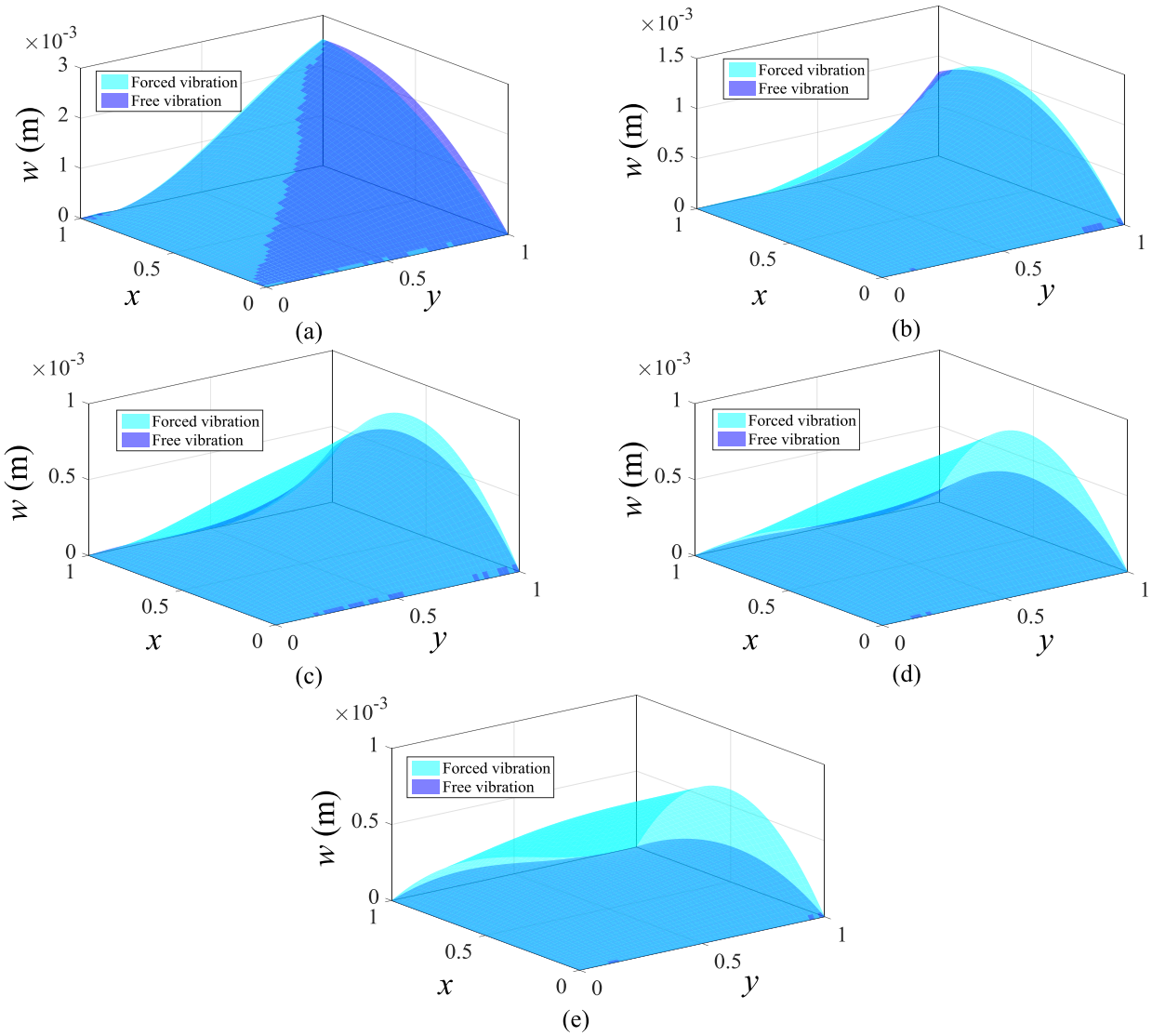

FIGURE 7. Maximum three-dimension deformations of FG plate at critical speed with different constraint positions. (a) Position 1. (b) Position 2. (c) Position 3. (d) Position 4. (e) Position 5.

closer to $y = 1$m (Edge 4), more area at Edge 3 is affected and finally, for Position 5, the maximum response reduces to 0.6mm. Note also that the deformation of the forced vibration almost overlaps with that of free vibration for Position 1. However, with the change of the position from 1 to 5, this difference is more obvious. As found in Table 7, the critical speed also increases from 20m/s to 50m/s when the local constraint moves from Position 1 to Position 5. The improvement

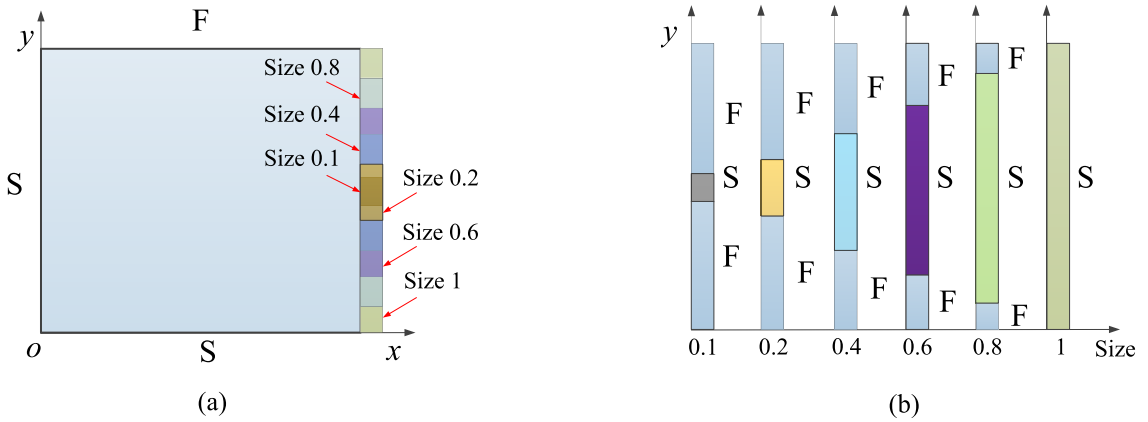

FIGURE 8. FG plate with SSXF. (a) Local constrained FG plate. (b) Constraints with different sizes (Edge 3).

TABLE 8. Maximum DAFs during forced vibration period and free vibration period for FG plate with five different local constraint sizes and M_r=1, p=2.

v_m	Size=0m (SSFF)		Size=0.1m		Size=0.2m		Size=0.4m		Size=0.6m		Size=0.8m		Size=1m (SSSF)	
(m/s)	Forced	Free	Forced	Free	Forced	Free	Forced	Free	Forced	Free	Forced	Free	Forced	Free
10	**5.2754**	**5.1436**	0.7102	0.1404	0.6769	0.1180	0.6418	0.0215	0.6345	0.0305	0.6411	0.0288	0.6549	0.0308
20	3.2315	4.1085	1.1542	0.6477	1.1270	0.5921	1.0951	0.5428	1.0871	0.5404	1.0988	0.5553	1.1236	0.5946
30	2.0744	3.3746	1.6360	1.3928	1.6023	1.3463	1.5316	1.2654	1.5175	1.2641	1.5518	1.2808	1.6178	1.3466
40	1.1240	2.6787	**2.0499**	2.1631	**2.1115**	2.2190	**2.1731**	2.2538	**2.1908**	2.2593	**2.2349**	2.3185	**2.3218**	2.4422
50	1.0584	2.7249	1.9040	**2.3186**	1.9801	**2.4708**	2.0980	2.6238	2.1427	2.6603	2.1764	2.7436	2.2341	2.9007
60	1.1539	2.9491	1.6327	2.2658	1.6756	2.4577	1.7528	**2.6747**	1.8041	**2.7370**	1.8330	**2.8414**	1.8765	**3.0148**
70	1.1766	2.4782	1.3549	2.1456	1.3799	2.3272	1.4025	2.5446	1.4257	2.6121	1.4474	2.7352	1.4791	2.9260
80	1.1480	1.7770	1.0826	1.9603	1.1079	2.1548	1.1094	2.3493	1.1099	2.4081	1.1238	2.5437	1.1454	2.7426
90	1.1038	1.3764	0.8474	1.7249	0.8775	1.9538	0.8777	2.1179	0.8711	2.1670	0.8797	2.3026	0.8933	2.4996

of the critical speed makes the inertia of the plate becomes more important, which in turn, enlarges the gap between the forced vibration and free vibration.

B. LOCAL CONSTRAINT WITH DIFFERENT SIZES

Similar as the analysis of the local constraints with different configuration positions, here, the local constraint with different configuration sizes is focused on. Fig. 8(a) shows the FG plate with SSXF boundary condition. It shows that six different configuration sizes are selected, namely 0.1m (Size 0.1), 0.2m (Size 0.2), 0.4m (Size 0.4), 0.6m (Size 0.6), 0.8m (Size 0.8), and 1m (Size 1), and all the local constraints are placed in the center area of Edge 3 ($x = 1$m). It should be mentioned that when the size equals to 0m (Size 0), the unconventional boundary condition is changed as classical boundary condition SSFF, while turns into SSSF when it equals to 1m. Fig. 8(b) depicts the constraint distribution along Edge 3 with different configuration sizes. It is clear that when the size increases, the area with free boundary condition declines while that with simple supported area becomes larger. The penalty parameters are listed in Table 2.

Figure 9 illustrates the transverse displacements, velocities and accelerations of center point of FG plate with SSXF boundary of five different configuration sizes. The mass ratio M_r is 1, power law index p is 2 and moving speed of mass v_m is 20m/s. It can be seen from these three diagrams that there is little difference for the displacements, velocities and accelerations during forced vibration period. For free vibration, the magnitude shows a small decrease with the increasing of the configuration size. However, an obvious phenomenon is that the corresponding phase of larger local constraint size advances. For example, in Fig. 9(a), the curve for larger size is relative in left side.

Tables 8 and 9 illustrate the relationships between SSXF of different sizes and maximum DAFs of the center point of FG plate with velocity varying from 10m/s to 90m/s. It is noted that the critical velocities for both force vibration period and free vibration period increase as the configuration size becomes larger. For example, in Table 9, the critical velocity for the first period of configuration Size 0 is 10m/s, while for configuration size from 0.1m to 1m, this velocity stabilizes at 40m/s. This trend is more obvious for the second period where the velocity increases from 10m/s to 60m/s. It is noted that the maximum DAFs for SSXF with configuration size from 0.1m to 1m share the similar value. However, when the velocity of moving mass is less than 30m/s, the maximum DAF of SSFF is significantly larger than those of other six configuration sizes. When this velocity is between 30m/s and 70m/s, this relationship changes and, finally, when the velocity exceeds 70m/s, the maximum DAF of SSFF is still in larger value. These changes are due to the increase of the critical velocity, which stands for the value beyond which the maximum DAF converges to a constant value.

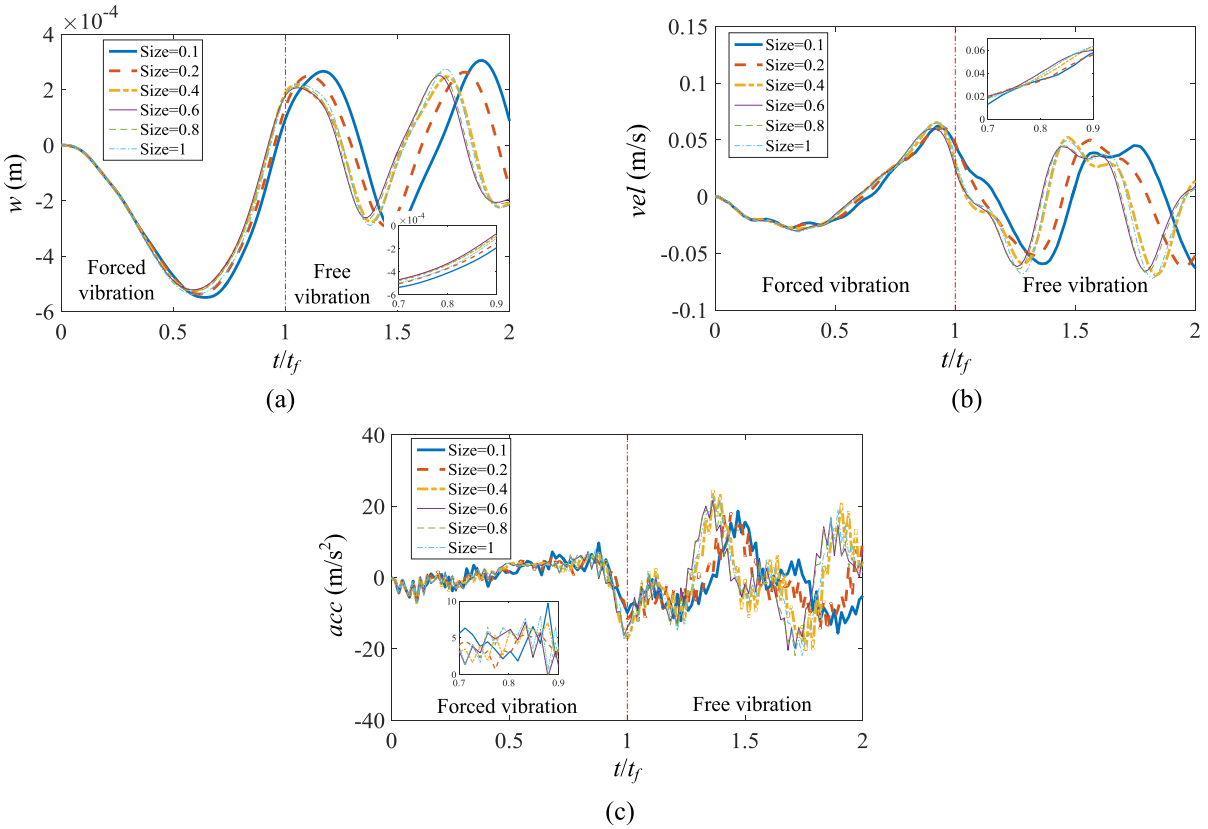

FIGURE 9. Responses of FG plate in z direction, with five different local constraint sizes, subjected to moving mass with M_r=1, p=2 and v_m=20m/s. (a) Displacement. (b) Velocity. (c) Acceleration.

TABLE 9. Maximum DAFs during forced vibration period and free vibration period for FG plate with five different local constraint sizes and M_r=0.2, p=2.

v_m	Size=0m (SSFF)		Size=0.1m		Size=0.2m		Size=0.4m		Size=0.6m		Size=0.8m		Size=1m (SSSF)	
(m/s)	Forced	Free	Forced	Free	Forced	Free	Forced	Free	Forced	Free	Forced	Free	Forced	Free
10	3.5261	3.5637	0.6615	0.1128	0.6655	0.1507	0.6749	0.1814	0.6889	0.1783	0.6975	0.1827	0.7089	0.1854
20	**4.2906**	**5.4353**	0.9252	0.2075	0.9034	0.0974	0.8827	0.0923	0.8779	0.1455	0.8882	0.1416	0.9084	0.1211
30	2.4546	4.1033	**0.9994**	0.7830	1.0102	0.7404	1.0316	0.6331	1.0468	0.6039	1.0605	0.6204	1.0808	0.6574
40	1.2449	3.0312	0.9716	**1.0234**	**1.0242**	0.8093	1.0943	0.9314	1.1282	0.9645	1.1462	0.9775	1.1697	1.0000
50	0.8103	2.3191	0.9461	1.0216	0.9950	**0.9852**	**1.1137**	1.0535	**1.1594**	1.0798	**1.1803**	1.1035	**1.2082**	1.1403
60	0.8009	2.1467	0.9495	0.9853	0.9735	0.9750	1.0797	**1.0854**	1.1448	**1.1453**	1.1674	**1.1695**	1.1968	**1.2015**
70	0.7853	2.0132	0.9268	0.9117	0.9933	0.9660	1.0356	1.0510	1.0850	1.1137	1.1064	1.1407	1.1372	1.1789
80	0.7653	1.6203	0.8561	0.8434	0.9942	0.9617	0.9923	1.0345	1.0128	1.0785	1.0297	1.1060	1.0589	1.1499
90	0.7410	0.9903	0.8024	0.8113	0.9543	0.9528	0.9357	1.0165	0.9365	1.0426	0.9484	1.0695	0.9727	1.1166

Therefore, at smaller velocity, the maximum DAF of SSFF is relatively larger.

Figure 10 illustrates the maximum three-dimension deformations of FG plate at critical speed with $M_r = 1$, $p = 2$. It also shows that the increase of the local constraint size has little influence on suppression of vibration. For example, when the size is 0.1m, the maximum deformation of this plate is 0.86mm, while 0.66mm for Size 1. Therefore, for purpose of vibration suppression, it is possible for local constraint to provide similar damping performance as conventional constraint. Another obvious result is that with increasing of the size, the difference between forced vibration and free vibration becomes larger. This is because the critical speed improves as the increase of the constraint size.

Fig. 11 illustrates the maximum deformations for different constraint sizes and positions in order to have a comprehensive comparison between the effects of configuration size and position. It can be seen that the local constraint position has more effect on the vibration suppression of SSXF plate. When the local constraint position is much closer to free edge, Edge 4 (such as Positions 3, 4, and 5), there is an obvious decrease in deformation no matter what the configuration size is (as shown in Fig. 11(b)).

C. SIMPLE SUPPORTED EDGE WITH LINEAR VARYING CONSTRAINT

Finally, another unconventional boundary condition is analyzed. In reality, it is quite often to find the triangular stiffened

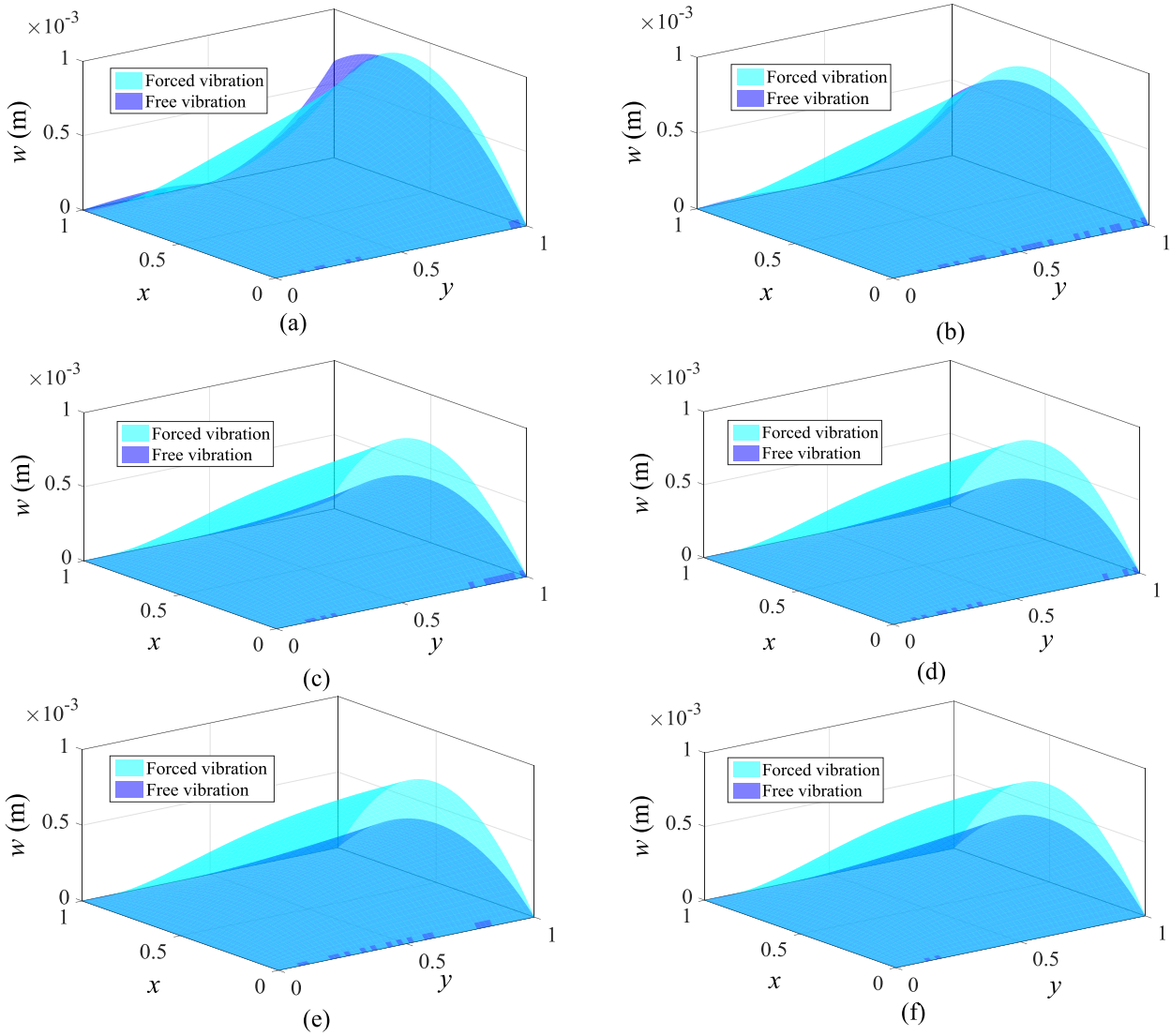

FIGURE 10. Maximum three-dimension deformations of FG plate at critical speed. (a) Size 0.1. (b) Size 0.2. (c) Size 0.4. (d) Size 0.6. (e) Size 0.8. (f) Size 1 (SSSF).

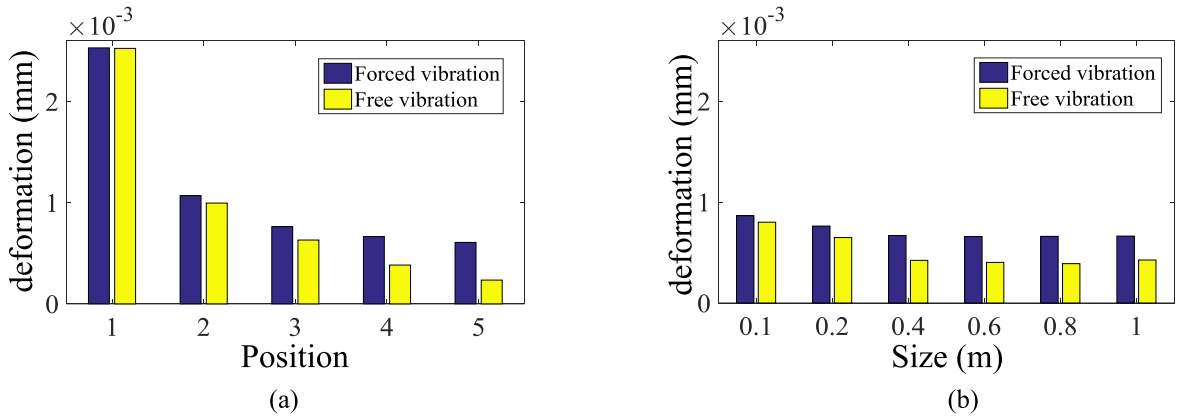

FIGURE 11. Effects of configuration position and configuration size on maximum deformations at critical speed. (a) Effect of configuration position. (b) Effect of configuration size.

plates are used to improve the strength characteristics of the load-bearing structure. As shown in Fig. 4(b), one edge of the FG plate is clamped in the fixed foundation while the adjacent edge is stiffened with a triangular plate. Due to the variation of the width of the triangular stiffened plate along the edge, it is rational to accept that one end of this edge is

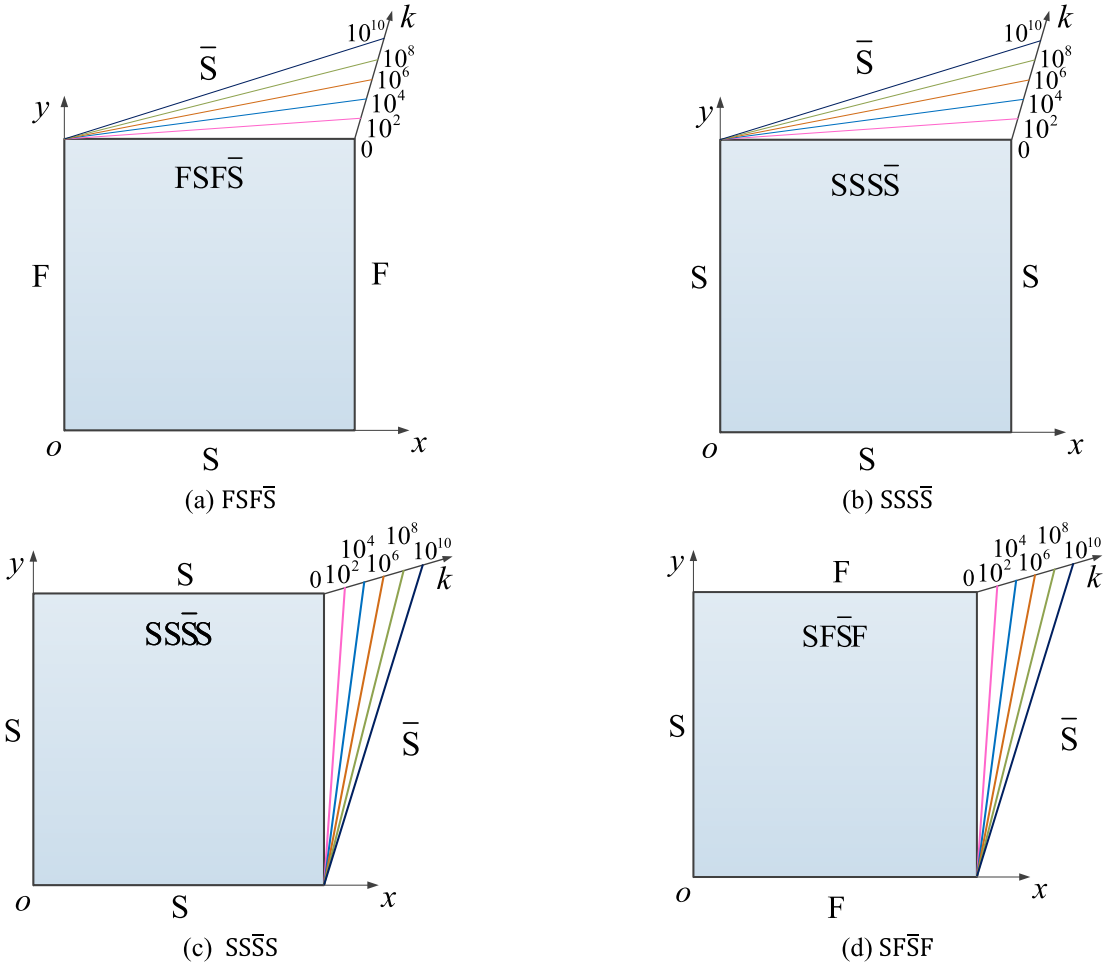

FIGURE 12. FG plate with four different boundary conditions. (a) FSFS̄. (b) SSSS̄. (c) SSS̄S. (d) SFS̄F.

clamped (C), while the opposite end of this edge is exposed to free boundary condition (F), which means the edge is totally restricted with varying constraint strength along this edge and different with the local constraint presented previously.

Without loss of generality, taking the Edge 3 ($x = 1$m) as an example, the point (1, 0) is subjected to simple supported boundary condition (S), while at point (1, 1), the boundary condition changes as free (F). For brevity, the symbol '$\bar{\text{S}}$' is used to represent this type of constraint, which means the boundary condition changes from S to F. Similarly, the symbol '$\bar{\text{C}}$' means it varies from C to F. Apparently, it is quite hard to find a suitable admissible function to satisfy this unconventional boundary condition. However, when it comes to the Penalty method, due to its unique advantage, this problem can be solved by changing the stiffness of the virtual springs along the edge considered. In this section, the constraint is assumed to vary linearly along the length and accordingly, the penalty parameters are as linear function of the position. Therefore, in (12), the $k_{,\mathrm{t}}J$ and $k_{,\mathrm{r}}^J$ are moved into the integral operations.

As shown in Fig. 12, four types of unconventional boundary conditions are considered, namely FSFS̄, SSSS̄, SSS̄S, and SFS̄F. The k-axis stands for the value of the penalty parameters and the solid line shows the variation of this value along the specific edge, where five variation ranges ($0 \sim k$) are selected: $0\sim10^2$, $0\sim10^4$, $0\sim10^6$, $0\sim10^8$, and $0\sim10^{10}$. The penalty parameters for the unconventional boundary condition $\bar{S}$ are listed in Table 2.

Figure 13 gives the center point DAF time history of the FG plate subjected to moving mass with $M_r = 1$, $v_m = 20$m/s, $p = 2$. For all those four boundary conditions, the DAFs are in higher value for smaller k. More specifically, when k is 10^2 and 10^4, the DAFs are almost identical with each other and in the maximum level. While for $k = 10^8$ and $k = 10^{10}$, the curves of the DAF also overlap with each other and its value is smaller than those of any other curves. This may because low penalty parameters (or stiffness of the virtual

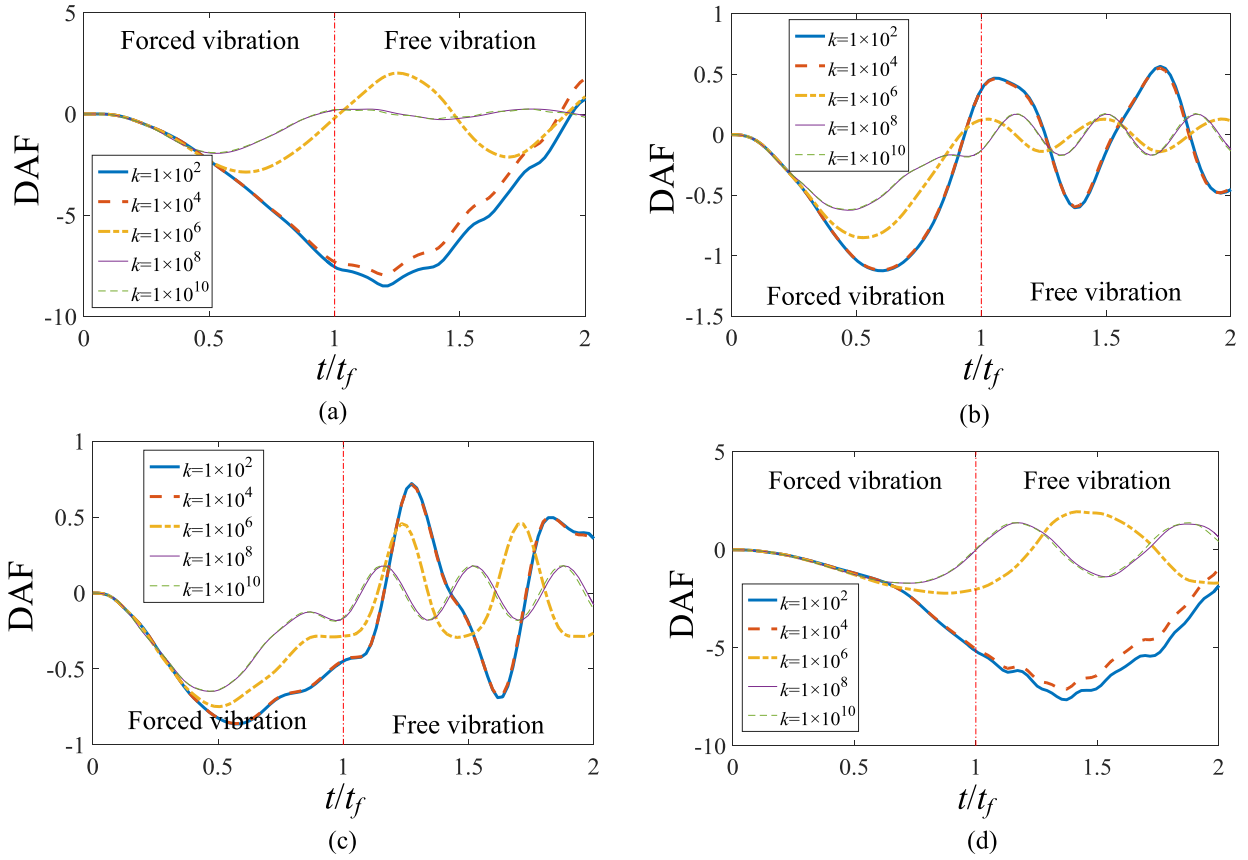

FIGURE 13. The DAF time history of center point of FG plate with different boundary conditions and M_r=1, v_m=20m/s, p=2. (a) FSF$\bar{S}$. (b) SSS$\bar{S}$. (c) SS$\bar{S}$S. (d) SF$\bar{S}$F.

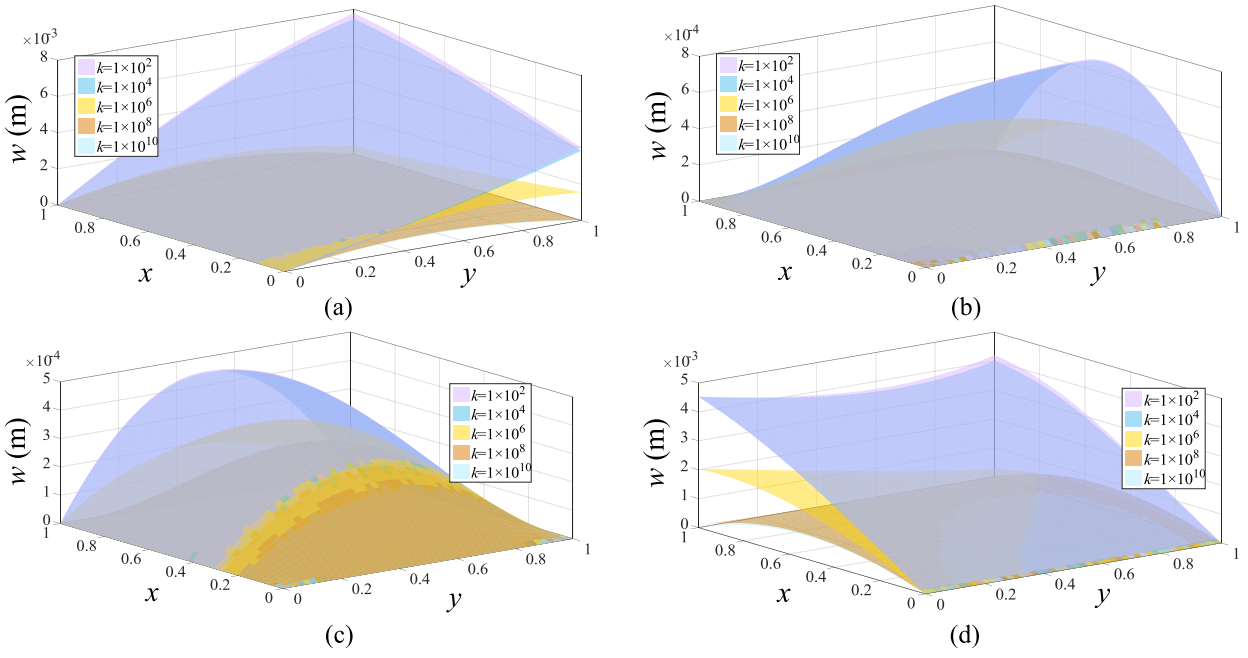

FIGURE 14. Maximum three-dimension deformations of FG plate subjected to moving mass with M_r=1, v_m=20m/s, p=2. (a) FSF$\bar{S}$. (b)SSS$\bar{S}$. (c) SS$\bar{S}$S. (d) SF$\bar{S}$F.

springs) provide weaker constraint strength. Another interesting thing is that, in the beginning, there is no difference between these responses and only after a certain time point, these curves begin to separate from each other. For these four figures, these normalized time points are 0.5253, 0.6667, 0.2828, and 0.3434, respectively. This is because for FSF$\bar{S}$

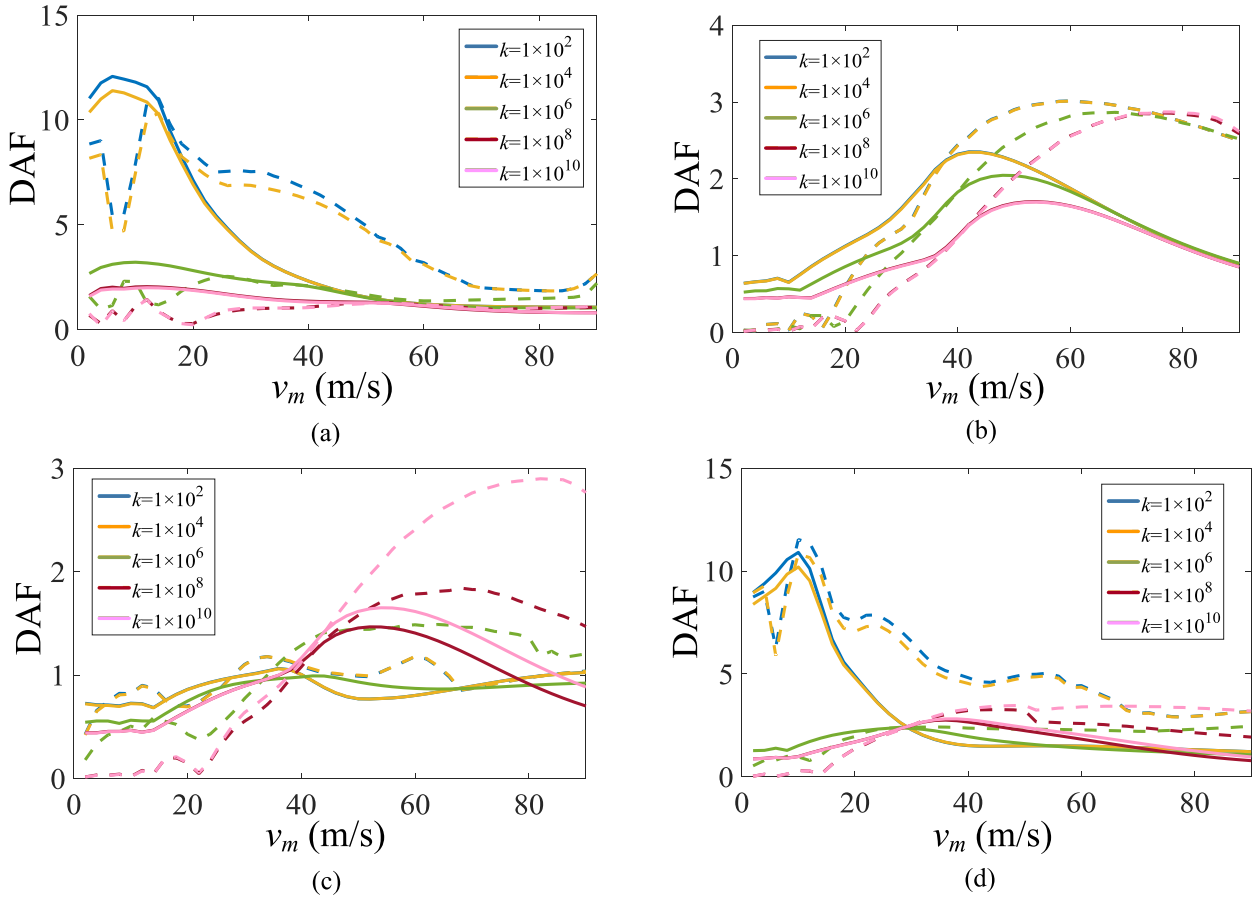

FIGURE 15. Variations of the absolute maximum DAF at the center of FG plate subjected to moving mass with M_r=1, v_m=20m/s, p=2. Solid line (—) for forced vibration. Dashed line (- - -) for free vibration. (a) FSF$\bar{\text{S}}$. (b) SSS$\bar{\text{S}}$. (c) SS$\bar{\text{S}}$S. (d) SFSF.

FG plate, the area affected by the constraint at Edge 3 ($\bar{\text{S}}$) is largest, which means it is faster to distinguish the response difference for different penalty parameters. On the contrary, the SF$\bar{\text{S}}$F FG plate has the smallest area affected by the unconventional constraint ($\bar{\text{S}}$) at Edge 3.

Figure 14 gives the three-dimension diagrams of maximum response of the FG plate subjected to moving mass $M_r = 1$, $v_m = 20$m/s, $p = 2$. It is clear to see that with smaller stiffness, the unconventional constrained edges have obvious deformation. However, when this value exceeds 10^8, these special constrained edges stable in the x-y plane, which also indicates it is reasonable to select the penalty parameters as 10^9 to deal with the fixed constraint.

Figure 15 shows the variations of the absolute maximum DAF at the center point of the FG plate subjected to moving mass with $M_r = 1$, $v_m = 20$m/s, $p = 2$. From the results given in Fig. 15, it is clear to see that with the increasing of the penalty parameters, the critical speeds of these FG plate for both forced vibration and free vibration also become faster. For example, for FSF$\bar{\text{S}}$ boundary condition, the critical speed increases from 10m/s to 36m/s as the penalty parameter, k, changes from 10^2 to 10^{10}, which results from the improvement of the stiffness of plate. However, it should be mentioned that for FSF$\bar{\text{S}}$, SF$\bar{\text{S}}$F, and SSS$\bar{\text{S}}$ plate, the DAFs show a decrease trend when the penalty parameter increases from 10^2 to 10^{10}. Nonetheless, for SS$\bar{\text{S}}$S plate, when the velocity exceeds 40m/s, the DAF of larger penalty parameter takes higher values. Therefore, the improvement of penalty parameter does not always lead to smaller maximum response.

The effect of boundary conditions on the dynamic responses of nonlinear FG plate has been extensively explored in this study. It was shown that the numerical procedure presented is capable of modeling nonlinear FG plate under moving mass with any arbitrary boundary conditions. It should be emphasized that using Penalty method to handle the troublesome arbitrary constraints eliminate the orthonormalization process for determining the admissible functions. Meanwhile, only one set of admissible functions is required for arbitrary boundary conditions. Additionally, the Newmark's constant acceleration method together with rank-one inverse Broyden quasi-Newton method is applied to guarantee the calculation stability and computational efficiency and accuracy of the numerical method.

V. CONCLUSIONS

A mixed method is proposed to evaluate the nonlinear response of FG plate with arbitrary boundary conditions under moving mass based on Rayleigh-Ritz solutions together with penalty method and Newmark with inverse Broyden quasi-Newton method. The pseudo-mass, pseudo-damping and pseudo-stiffness effects are obviously presented to feature the all inertial effects of moving mass in governing equation of motion of system. The present method has two main advantages, one is that is can deal with arbitrary boundary conditions using only one set of admissible functions, and exclude the orthonormalization process widely used in other methods, such as eigenfunction expansion method and BCOPs. The other is that Newmark's time integration together with rank-one inverse Broyden quasi-Newton method is adopted, which is of more computational efficiency than the commonly used Broyden quasi-Newton method and Newton–Raphson method, to solve the nonlinear coupled differential equations of second-order in time. Meanwhile, the numerical instability can be effectively avoided through choosing the appropriate time increments and iterative solution procedure. The comparison and convergence studies are performed to check the accuracy and efficacy of the present technique.

Additionally, parametric studies are carried out to reveal the effects of material distribution, velocity of moving mass and different boundary conditions on the nonlinear responses of FG plates. The following points can be outlined from the present study:

(1) It is unreasonable to neglect the free vibration of FG plate under moving load, because the critical velocity of free vibration is always not smaller than that of forced vibration.

(2) For classical boundary conditions, smaller constraints always result in lower critical speed for the forced vibration of FG plate. For local constraints, the closer the simple boundary condition is to the free edge, the higher capacity of vibration suppression it can perform, and the higher value of the critical velocity is both for free vibration and forced vibration.

(3) When configured in the central area of the edge of FG plate, the constraint size has little influence on the magnitude of the nonlinear response. However, an obvious trend is that the critical velocity always rises as the increasing of the constraint size.

(4) For local constraints, the influence of the constraint position is much higher than that of constraints size. Therefore, proper local constraint can also meet the need of vibration mitigation.

(5) For linear varying constraint, increasing the penalty parameter can effectively damp the nonlinear response of the FG plate. However, the influences of penalty parameter on the critical speeds for free vibration and forced vibration are determined by the specific boundary condition.

APPENDIX

The sub-matrices of mass matrix $\mathbf{M}$ are expressed as

$$\begin{aligned}
M_{11}^{(u,v)} &= I_0 E_{(0,0)}^{(m,n)} F_{(0,0)}^{(i,j)} + I_2 E_{(1,1)}^{(m,n)} F_{(0,0)}^{(i,j)} + I_2 E_{(0,0)}^{(m,n)} F_{(1,1)}^{(i,j)} \\
M_{12}^{(u,v)} &= M_{13}^{(u,v)} = M_{21}^{(v,u)} = M_{31}^{(v,u)} = -I_1 E_{(1,0)}^{(m,n)} F_{(0,0)}^{(i,j)} \\
M_{22}^{(u,v)} &= M_{33}^{(u,v)} = I_0 E_{(0,0)}^{(m,n)} F_{(0,0)}^{(i,j)} \qquad \text{(A.1)} \\
M_{11}^{*(u,v)} &= M \phi_m(x_0) \phi_n(x_0) \varphi_i(y_0) \varphi_j(y_0) \qquad \text{(A.2)}
\end{aligned}$$

where $u = (m-1) \times N + i$, $v = (n-1) \times N + j$, $i = 1, 2, \ldots, N$ and $j = 1, 2, \ldots, N$. In the following expressions, this relationship is also satisfied.

The matrices $E_{(0,0)}^{(m,n)}$ and $F_{(0,0)}^{(i,j)}$ are constructed by

$$\begin{aligned}
E_{(s,t)}^{(m,n)} &= \int_0^L \frac{\partial^s \phi_m(x)}{\partial x^s} \frac{\partial^t \phi_n(x)}{\partial x^t} dy \quad \text{and} \\
F_{(s,t)}^{(i,j)} &= \int_0^L \frac{\partial^s \varphi_m(y)}{\partial y^s} \frac{\partial^t \varphi_n(y)}{\partial y^t} dy \qquad \text{(A.3)}
\end{aligned}$$

which is also suitable for the construction of similar matrices in the following expressions.

The sub-matrices of damping matrix $\mathbf{C}$ are expressed as

$$\begin{aligned}
C_{11}^{*(u,v)} &= 2M\dot{x}_0 \phi_m(x_0) \frac{\partial \phi_n(x_0)}{\partial x_0} \varphi_i(y_0) \varphi_j(y_0) \\
&\quad + 2M\dot{y}_0 \phi_m(x_0) \phi_n(x_0) \varphi_i(y_0) \frac{\partial \varphi_j(y_0)}{\partial y_0} \qquad \text{(A.4)}
\end{aligned}$$

The sub-matrices of linear stiffness matrix $\mathbf{K}$ are expressed as

$$\begin{aligned}
K_{11}^{(u,v)} &= E_2 \begin{pmatrix} E_{(2,2)}^{(m,n)} F_{(0,0)}^{(i,j)} + E_{(0,0)}^{(m,n)} F_{(2,2)}^{(i,j)} + 2(1-\mu) \\ E_{(1,1)}^{(m,n)} F_{(1,1)}^{(i,j)} + \mu \left(E_{(0,2)}^{(m,n)} F_{(2,0)}^{(i,j)} + E_{(2,0)}^{(m,n)} F_{(0,2)}^{(i,j)} \right) \end{pmatrix} \\
&\quad + P_w^{(u,v)} \\
K_{12}^{(u,v)} &= K_{21}^{(v,u)} = -E_1 \left(E_{(2,1)}^{(m,n)} F_{(0,0)}^{(i,j)} + \mu E_{(0,1)}^{(m,n)} F_{(2,0)}^{(i,j)} \right. \\
&\quad \left. + (1-\mu) E_{(1,0)}^{(m,n)} F_{(1,1)}^{(i,j)} \right) \\
K_{13}^{(u,v)} &= K_{31}^{(v,u)} = -E_1 \left(E_{(0,0)}^{(m,n)} F_{(2,1)}^{(i,j)} + \mu E_{(2,0)}^{(m,n)} F_{(2,1)}^{(i,j)} \right. \\
&\quad \left. + (1-\mu) E_{(1,1)}^{(m,n)} F_{(1,0)}^{(i,j)} \right) \\
K_{22}^{(u,v)} &= E_0 \left(E_{(1,1)}^{(m,n)} F_{(0,0)}^{(i,j)} + \frac{(1-\mu)}{2} E_{(0,0)}^{(m,n)} F_{(1,1)}^{(i,j)} \right) + P_p^{(u,v)} \\
K_{23}^{(u,v)} &= E_0 \left(\mu E_{(1,0)}^{(m,n)} F_{(0,1)}^{(i,j)} + \frac{(1-\mu)}{2} E_{(0,1)}^{(m,n)} F_{(1,0)}^{(i,j)} \right) \\
K_{33}^{(u,v)} &= E_0 \left(E_{(0,0)}^{(m,n)} F_{(1,1)}^{(i,j)} + \frac{(1-\mu)}{2} E_{(1,1)}^{(m,n)} F_{(0,0)}^{(i,j)} \right) + P_q^{(u,v)} \qquad \text{(A.5)} \\
K_{11}^{*(u,v)} &= 2M\dot{x}_0\dot{y}_0 \left(\frac{\partial \phi_m(x_0)}{\partial x_0} \phi_n(x_0) \frac{\partial \varphi_i(y_0)}{\partial y_0} \varphi_j(y_0) \right. \\
&\quad \left. + \phi_m(x_0) \frac{\partial \phi_n(x_0)}{\partial x_0} \varphi_i(y_0) \frac{\partial \varphi_j(y_0)}{\partial y_0} \right) \\
&\quad + M\dot{x}_0^2 \left(\frac{\partial^2 \phi_m(x_0)}{\partial x_0^2} \phi_n(x_0) \varphi_i(y_0) \varphi_j(y_0) \right.
\end{aligned}$$

$$
\begin{aligned}
K_{11}^{NL(u,v)} &= \frac{1}{2}E_0\int_0^L\int_0^W \left(w_{,x}^2 e_{(1,1)}^{(m,n)} f_{(0,0)}^{(i,j)} + w_{,y}^2 e_{(0,0)}^{(m,n)} f_{(1,1)}^{(i,j)} + w_{,x}^2 e_{(0,0)}^{(m,n)} f_{(1,1)}^{(i,j)} + w_{,y}^2 e_{(1,1)}^{(m,n)} f_{(0,0)}^{(i,j)}\right) dxdy \\
&\quad - \frac{1}{2}E_1\int_0^L\int_0^W \begin{pmatrix} w_{,x} e_{(2,1)}^{(m,n)} f_{(0,0)}^{(i,j)} + 2w_{,xx} e_{(1,1)}^{(m,n)} f_{(0,0)}^{(i,j)} + w_{,y} e_{(0,0)}^{(m,n)} f_{(2,1)}^{(i,j)} + 2w_{,yy} e_{(0,0)}^{(m,n)} f_{(1,1)}^{(i,j)} \\ +2(1-\mu)\left(w_{,x} e_{(1,0)}^{(m,n)} f_{(1,1)}^{(i,j)} + w_{,y} e_{(1,1)}^{(m,n)} f_{(0,1)}^{(i,j)} + w_{,xy} e_{(0,1)}^{(m,n)} f_{(1,0)}^{(i,j)}\right) \\ +2\mu w_{,xx} e_{(0,0)}^{(m,n)} f_{(1,1)}^{(i,j)} + \mu w_{,y} e_{(2,0)}^{(m,n)} f_{(0,1)}^{(i,j)} + 2\mu w_{,yy} e_{(1,1)}^{(m,n)} f_{(0,0)}^{(i,j)} + \mu w_{,x} e_{(0,1)}^{(m,n)} f_{(2,0)}^{(i,j)} \end{pmatrix} dxdy \\
K_{21}^{NL(u,v)} &= \frac{E_0}{2}\int_0^L\int_0^W \left(w_{,x} e_{(1,1)}^{(m,n)} f_{(0,0)}^{(i,j)} + (1-\mu) w_{,x} e_{(0,0)}^{(m,n)} f_{(1,1)}^{(i,j)} + \mu w_{,y} e_{(1,0)}^{(m,n)} f_{(0,1)}^{(i,j)}\right) dxdy \\
K_{31}^{NL(u,v)} &= \frac{E_0}{2}\int_0^L\int_0^W \left(w_{,y} e_{(0,0)}^{(m,n)} f_{(1,1)}^{(i,j)} + (1-\mu) w_{,y} e_{(1,1)}^{(m,n)} f_{(0,0)}^{(i,j)} + \mu w_{,x} e_{(0,1)}^{(m,n)} f_{(1,0)}^{(i,j)}\right) dxdy
\end{aligned} \tag{A.8}
$$

$$
\begin{aligned}
&\quad + \phi_m(x_0)\frac{\partial^2\phi_n(x_0)}{\partial x_0^2}\varphi_i(y_0)\varphi_j(y_0)\Bigg) \\
&+ M\dot{y}_0^2\left(\phi_m(x_0)\phi_n(x_0)\frac{\partial^2\varphi_i(y_0)}{\partial y_0^2}\varphi_j(y_0)\right. \\
&\quad \left. + \phi_m(x_0)\phi_n(x_0)\varphi_i(y_0)\frac{\partial^2\varphi_j(y_0)}{\partial y_0^2}\right)
\end{aligned} \tag{A.6}
$$

and $P_J^{(u,v)}$, $J = w, p, q$, is defined as

$$
P_J^{(u,v)} = \frac{1}{2}\begin{bmatrix}
\phi_m(0)\phi_n(0)\int_0^W k_{1,t}^J(y)\varphi_i(y)\varphi_j(y)dy \\
+\phi_{m,x}(0)\phi_{n,x}(0)\int_0^W k_{1,r}^J(y)\varphi_i(y)\varphi_j(y)dy \\
+\varphi_i(0)\varphi_j(0)\int_0^L k_{2,t}^J(y)\varphi_i(y)\varphi_j(y)dx \\
+\varphi_{i,y}(0)\varphi_{j,y}(0)\int_0^L k_{2,r}^J(y)\varphi_i(y)\varphi_j(y)dx \\
+\phi_m(L)\phi_n(L)\int_0^W k_{3,t}^J(y)\varphi_i(y)\varphi_j(y)dy \\
+\phi_{m,x}(L)\phi_{n,x}(L)\int_0^W k_{3,r}^J(y)\varphi_i(y)\varphi_j(y)dy \\
+\varphi_i(W)\varphi_j(W)\int_0^L k_{4,t}^J(y)\varphi_i(y)\varphi_j(y)dx \\
+\varphi_{i,y}(W)\varphi_{j,y}(W)\int_0^L k_{4,r}^J(y)\varphi_i(y)\varphi_j(y)dx
\end{bmatrix} \tag{A.7}
$$

The sub-matrices of nonlinear stiffness matrix $\mathbf{K}^{NL}$ are expressed as (A.8), as shown at the top of this page.

The matrices $e_{(0,0)}^{(m,n)}$ and $f_{(0,0)}^{(i,j)}$ are constructed by

$$
e_{(s,t)}^{(m,n)} = \frac{\partial^s\phi_m(x)}{\partial x^s}\frac{\partial^t\phi_n(x)}{\partial x^t} \text{ and } f_{(s,t)}^{(i,j)} = \frac{\partial^s\varphi_m(y)}{\partial y^s}\frac{\partial^t\varphi_n(y)}{\partial y^t} \tag{A.9}
$$

The sub-vector of non-zero part of force vector $\{Q\}$ is expressed as

$$
f^u = -Mg\phi_m(x(t))\varphi_i(y_0) \tag{A.10}
$$

REFERENCES

[1] D. K. Jha, T. Kant, and R. K. Singh, "A critical review of recent research on functionally graded plates," *Compos. Struct.*, vol. 96, no. 4, pp. 833–849, 2013.

[2] W. Zhou, H. Zhou, R. Zhang, Y. Pei, and D. Fang, "Measuring residual stress and its influence on properties of porous ZrO_2/(ZrO_2+Ni) ceramics," *Mater. Sci. Eng., A*, vol. 622, pp. 82–90, Jan. 2015.

[3] W. Zhou, R. Zhang, and D. Fang, "Design and analysis of the porous ZrO_2/(ZrO_2+Ni) ceramic joint with load bearing–heat insulation integration," *Ceramics Int.*, vol. 42, no. 1, pp. 1416–1424, 2016.

[4] M. Yamaguchi, "III–V compound multi-junction solar cells: Present and future," *Solar Energy Mater. Solar Cells*, vol. 75, nos. 1–2, pp. 261–269, 2003.

[5] M. Bahraminasab, B. B. Sahari, K. L. Edwards, F. Farahmand, and M. Arumugam, "Aseptic loosening of femoral components—Materials engineering and design considerations," *Mater Des.*, vol. 44, pp. 155–163, Feb. 2013.

[6] T.-T. Nguyen, N.-I. Kim, and J. Lee, "Free vibration of thin-walled functionally graded open-section beams," *Compos. B, Eng.*, vol. 95, pp. 105–116, Jun. 2016.

[7] Z.-H. Wang, X.-H. Wang, G.-D. Xu, S. Cheng, and T. Zeng, "Free vibration of two-directional functionally graded beams," *Compos. Struct.*, vol. 135, pp. 191–198, Jan. 2016.

[8] A. H. Baferani, A. R. Saidi, and E. Jomehzadeh, "An exact solution for free vibration of thin functionally graded rectangular plates," *Proc. Inst. Mech. Eng. C, J. Mech. Eng. Sci.*, vol. 225, no. 3, pp. 526–536, 2010.

[9] J. L. Mantari, I. A. Ramos, E. Carrera, and M. Petrolo, "Static analysis of functionally graded plates using new non-polynomial displacement fields via Carrera unified formulation," *Compos. B, Eng.*, vol. 89, pp. 127–142, Mar. 2016.

[10] J. L. Mantari and E. V. Granados, "Dynamic analysis of functionally graded plates using a novel FSDT," *Compos. B, Eng.*, vol. 75, pp. 148–155, Jun. 2015.

[11] S. S. Akavci and A. H. Tanrikulu, "Static and free vibration analysis of functionally graded plates based on a new quasi-3D and 2D shear deformation theories," *Compos. B, Eng.*, vol. 83, pp. 203–215, Dec. 2015.

[12] M. Şimşek, "Non-linear vibration analysis of a functionally graded Timoshenko beam under action of a moving harmonic load," *Compos. Struct.*, vol. 92, no. 10, pp. 2532–2546, 2010.

[13] S. Taeprasartsit, "Nonlinear free vibration of thin functionally graded beams using the finite element method," *J. Vib. Control*, vol. 21, no. 1, pp. 29–46, 2015.

[14] M. Şimşek, "Vibration analysis of a functionally graded beam under a moving mass by using different beam theories," *Compos. Struct.*, vol. 92, no. 4, pp. 904–917, 2010.

[15] M. Şimşek, T. Kocatürk, and Ş. D. Akbaş, "Dynamic behavior of an axially functionally graded beam under action of a moving harmonic load," *Compos. Struct.*, vol. 94, no. 8, pp. 2358–2364, 2012.

[16] H. Deng and W. Cheng, "Dynamic characteristics analysis of bi-directional functionally graded Timoshenko beams," *Compos. Struct.*, vol. 141, pp. 253–263, May 2016.

[17] A. H. Akbarzadeh *et al.*, "Mechanical behaviour of functionally graded plates under static and dynamic loading," *Proc. Inst. Mech. Eng. C, J. Mech. Eng. Sci.*, vol. 225, no. 2, pp. 326–333, 2011.

[18] M. Ruan and Z.-M. Wang, "Transverse vibrations of moving skew plates made of functionally graded material," *J. Vib. Control*, vol. 22, no. 16, pp. 3504–3517, 2016.

[19] P. Malekzadeh and S. M. Monajjemzadeh, "Nonlinear response of functionally graded plates under moving load," *Thin-Walled Struct.*, vol. 96, pp. 120–129, Nov. 2015.

[20] A. Mamandi, R. Mohsenzadeh, and M. H. Kargarnovin, "Nonlinear dynamic analysis of a rectangular plate subjected to accelerated/decelerated moving load," *J. Theor. Appl. Mech.*, vol. 53, no. 1, pp. 151–166, 2015.

[21] M. Rafiee, M. Mohammadi, B. S. Aragh, and H. Yaghoobi, "Nonlinear free and forced thermo-electro-aero-elastic vibration and dynamic response of piezoelectric functionally graded laminated composite shells: Part II: Numerical results," *Compos. Struct.*, vol. 103, no. 9, pp. 188–196, 2013.
[22] D. H. Bich and N. X. Nguyen, "Nonlinear vibration of functionally graded circular cylindrical shells based on improved Donnell equations," *J. Sound Vib.*, vol. 331, no. 25, pp. 5488–5501, 2012.
[23] P. Malekzadeh and S. M. Monajjemzadeh, "Dynamic response of functionally graded plates in thermal environment under moving load," *Compos. B, Eng.*, vol. 45, no. 1, pp. 1521–1533, 2013.
[24] J. Yang and H.-S. Shen, "Vibration characteristics and transient response of shear-deformable functionally graded plates in thermal environments," *J. Sound Vib.*, vol. 255, no. 3, pp. 579–602, 2002.
[25] X.-L. Huang and H.-S. Shen, "Nonlinear vibration and dynamic response of functionally graded plates in thermal environments," *Int. J. Solids Struct.*, vol. 41, nos. 9–10, pp. 2403–2427, 2004.
[26] F. R. Rofooei, A. Enshaeian, and A. Nikkhoo, "Dynamic response of geometrically nonlinear, elastic rectangular plates under a moving mass loading by inclusion of all inertial components," *J. Sound Vib.*, vol. 394, pp. 497–514, Apr. 2017.
[27] M. M. Najafizadeh, J. Mohammadi, and P. Khazaeinejad, "Vibration characteristics of functionally graded plates with non-ideal boundary conditions," *Mech. Adv. Mater. Struct.*, vol. 19, no. 7, pp. 543–550, 2012.
[28] S. S. Akavci, "An efficient shear deformation theory for free vibration of functionally graded thick rectangular plates on elastic foundation," *Compos. Struct.*, vol. 108, pp. 667–676, Feb. 2014.
[29] S. S. Akavci, "Mechanical behavior of functionally graded sandwich plates on elastic foundation," *Compos. B, Eng.*, vol. 96, pp. 136–152, Jul. 2016.
[30] S. A. Sheikholeslami and A. R. Saidi, "Vibration analysis of functionally graded rectangular plates resting on elastic foundation using higher-order shear and normal deformable plate theory," *Compos. Struct.*, vol. 106, pp. 350–361, Dec. 2013.
[31] M. Şimşek and S. Cansız, "Dynamics of elastically connected double-functionally graded beam systems with different boundary conditions under action of a moving harmonic load," *Compos. Struct.*, vol. 94, pp. 2861–2878, Sep. 2012.
[32] M. S. Sari and E. A. Butcher, "Free vibration analysis of non-rotating and rotating Timoshenko beams with damaged boundaries using the Chebyshev collocation method," *Int. J. Mech. Sci.*, vol. 60, no. 1, pp. 1–11, 2012.
[33] N. Wattanasakulpong and Q. Mao, "Dynamic response of Timoshenko functionally graded beams with classical and non-classical boundary conditions using Chebyshev collocation method," *Compos. Struct.*, vol. 119, pp. 346–354, Jan. 2015.
[34] A. Gupta, M. Talha, and B. N. Singh, "Vibration characteristics of functionally graded material plate with various boundary constraints using higher order shear deformation theory," *Compos. B, Eng.*, vol. 94, pp. 64–74, Jun. 2016.
[35] A. Enshaeian and F. R. Rofooei, "Geometrically nonlinear rectangular simply supported plates subjected to a moving mass," *Acta Mech.*, vol. 225, pp. 595–608, Feb. 2014.
[36] S. Ilanko and G. K. Bharathy, "Positive and negative penalty parameters in optimisation subjected to continuous constraints," *Comput. Struct.*, vols. 108–109, pp. 83–92, Oct. 2012.
[37] Q. Song, J. Shi, Z. Liu, and Y. Wan, "Dynamic analysis of rectangular thin plates of arbitrary boundary conditions under moving loads," *Int. J. Mech. Sci.*, vol. 117, pp. 16–29, Oct. 2016.
[38] S. Chakraverty. *Vibration of Plates*. Boca Raton, FL, USA: CRC Press, 2009.
[39] S. Schlenkrich and A. Walther, "Global convergence of quasi-Newton methods based on adjoint Broyden updates," *Appl. Numer. Math.*, vol. 59, pp. 1120–1136, May 2009.
[40] L. Frýba, *Vibration of Solids and Structures Under Moving Loads*. London, U.K.: Thomas Telford House, 1999.
[41] D. J. Gorman, "An exact analytical approach to the free vibration analysis of rectangular plates with mixed boundary conditions," *J. Sound Vib.*, vol. 93, no. 2, pp. 235–247, 1984.
[42] P. A. A. Laura and R. O. Gross, "Transverse vibrations of rectangular plates with edges elastically restrained against translation and rotation," *J. Sound Vib.*, vol. 75, pp. 101–107, Mar. 1981.
[43] K. M. Liew, K. C. Hung, and M. K. Lim, "Roles of domain decomposition method in plate vibrations: Treatment of mixed discontinuous periphery boundaries," *Int. J. Mech. Sci.*, vol. 35, no. 7, pp. 615–632, 1993.
[44] F.-L. Liu and K. M. Liew, "Analysis of vibrating thick rectangular plates with mixed boundary constraints using differential quadrature element method," *J. Sound Vib.*, vol. 225, no. 5, pp. 915–934, 1999.
[45] M. Malik and C. W. Bert, "Implementing multiple boundary conditions in the DQ solution of higher-order PDEs: Application to free vibration of plates," *Int. J. Numer. Methods Eng.*, vol. 39, pp. 1237–1258, Apr. 1996.

QINGHUA SONG received the B.S., M.S., and Ph.D. degrees in mechanical engineering from Shandong University, Ji'nan, China, in 1999, 2003, and 2009, respectively. He was a Visiting Scholar with Virginia Tech University, in 2015.

From 2009 to 2011, he was a Post-Doctoral Fellow with the School of Materials Science and Engineering, Shandong University. From 2011 to 2015, he was a Lecturer with the School of Mechanical Engineering, Shandong University, where he has been an Associate Professor since 2015. His research interests include the structural vibration and control, (micro) cutting system dynamics, micro process equipment technology, and biomedical machinery.

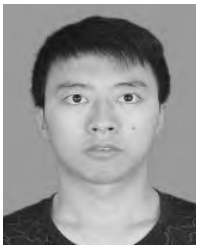

YUN QIN received the B.S. degrees in mechanical engineering from Shandong University, Ji'nan, China, in 2018, where he is currently pursuing the M.S. degree.

His research interests include mechanical properties and vibration control of composite materials.

ZHANQIANG LIU received the B.S. and M.S. degrees in mechanical engineering from Shandong University, Ji'nan, China, in 1994, and the Ph.D. degree in philosophy from the City University of Hong Kong, Hong Kong, in 1999.

From 1999 to 2001, he was a Post-Doctoral Fellow with the School of Mechanical Engineering, Shandong University. From 2001 to 2002, he was an Associate Professor with the School of Mechanical Engineering, Shandong University, where he has been a Professor since 2002. His research interests include machining theory and tool technology. He is a member of ASME and the Executive Director of the China Metal Cutting Tool Association.

Dr. Liu has received the Second Prize of the Natural Science of the Ministry of Education in 2005, the Second Prize of the Shandong Science and Technology Progress Award in 2008, and the Second Prize of the National Defense Science and Technology Progress in 2012.

JIAHAO SHI received the B.S. and M.S. degrees in mechanical engineering from Shandong University, Ji'nan, China, in 2014 and 2017, respectively. He currently pursuing the Ph.D. degree with McGill University, Montreal, Canada.

His research interests include plate vibration control and vibration signal analysis.

BING WANG received the B.S. and Ph.D. degrees in mechanical engineering from Shandong University, Ji'nan, China, in 2011 and 2016, respectively. He is currently pursuing the joint Ph.D. degree with the Department of Mechanical Engineering, Michigan State University.

Since 2017, he has been a Post-Doctoral Fellow with the School of Materials Science and Engineering, Shandong University. His research interests include vibration control and tool design.